RADC-TR-89-229
Annual Report
November 1989

SIGNAL PROCESSING DEVELOPMENT

Parke Mathematical Laboratories, Incorporated

T.B. Barrett, R. Marshall, J. Bloom, C. Comer, J. Caulfield, C. Warde, M. Salour

ROME AIR DEVELOPMENT CENTER
Air Force Systems Command
Griffiss Air Force Base, NY 13441-5700

This report has been reviewed by the RADC Public Affairs Division (PA) and is releasable to the National Technical Information Service (NTIS). At NTIS it will be releasable to the general public, including foreign nations.

RADC-TR-89-229 has been reviewed and is approved for publication.

APPROVED: 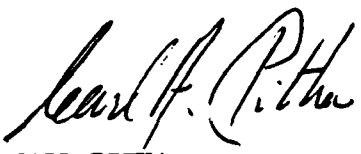

CARL PITHA
Project Engineer

APPROVED: 

HAROLD ROTH
Director of Solid State Sciences

FOR THE COMMANDER: 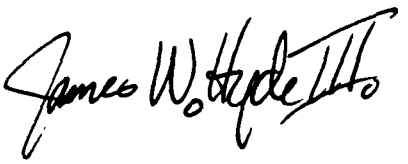

JAMES W. HYDE III
Directorate of Plans & Programs

If your address has changed or if you wish to be removed from the RADC mailing list, or if the addressee is no longer employed by your organization, please notify RADC (ESO) Hanscom AFB MA 01731-5000. This will assist us in maintaining a current mailing list.

Do not return copies of this report unless contractual obligations or notices on a specific document require that it be returned.

UNCLASSIFIED

SECURITY CLASSIFICATION OF THIS PAGE

REPORT DOCUMENTATION PAGE

Form Approved OMB No. 0704-0188

1a. REPORT SECURITY CLASSIFICATION UNCLASSIFIED	1b. RESTRICTIVE MARKINGS N/A
2a. SECURITY CLASSIFICATION AUTHORITY N/A	3. DISTRIBUTION/AVAILABILITY OF REPORT Approved for public release; distribution unlimited.
2b. DECLASSIFICATION/DOWNGRADING SCHEDULE N/A	
4. PERFORMING ORGANIZATION REPORT NUMBER(S) N/A	5. MONITORING ORGANIZATION REPORT NUMBER(S) RADC-TR-89-229
6a. NAME OF PERFORMING ORGANIZATION Parke Mathematical Laboratories, Incorporated 6b. OFFICE SYMBOL (If applicable)	7a. NAME OF MONITORING ORGANIZATION Rome Air Development Center (ESO)
6c. ADDRESS (City, State, and ZIP Code) One River Road Carlisle MA 01741	7b. ADDRESS (City, State, and ZIP Code) Hanscom AFB MA 01731-5000
8a. NAME OF FUNDING/SPONSORING ORGANIZATION Rome Air Development Center 8b. OFFICE SYMBOL (If applicable) ESO	9 PROCUREMENT INSTRUMENT IDENTIFICATION NUMBER F19628-84-C-0008
8c. ADDRESS (City, State, and ZIP Code) Hanscom AFB MA 01731-5000	10. SOURCE OF FUNDING NUMBERS PROGRAM ELEMENT NO. 62702F; PROJECT NO. 4600; TASK NO 19; WORK UNIT ACCESSION NO 49

11. TITLE (Include Security Classification)

SIGNAL PROCESSING DEVELOPMENT

12. PERSONAL AUTHOR(S)

T. B. Barrett, R. Marshall, J. Bloom, C. Comer, J. Caulfield, C. Warde, M. Salour

13a. TYPE OF REPORT	13b. TIME COVERED	14. DATE OF REPORT (Year, Month, Day)	15. PAGE COUNT
Annual	FROM Jan 84 TO Dec 84	November 1989	102

16. SUPPLEMENTARY NOTATION

N/A

17. COSATI CODES			18. SUBJECT TERMS (Continue on reverse if necessary and identify by block number)
FIELD	GROUP	SUB-GROUP	Platinum silicide; Indium phosphide; Matrix partition; Holography; Ray tracing
20	02		
20	06		

19. ABSTRACT (Continue on reverse if necessary and identify by block number)

The electron microscope has been applied to the study of the growth of thin epitaxial films on silicon substrates. The study of the nature of platinum-silicide films formed by heating evaporated platinum films on these substrates is discussed.

The use of ultra high vacuum systems together with a residual gas analyzer (RGA) is discussed as they relate to the preparation of silicides, a dielectric layer of silicon monoxide is evaporated and an ion beam implanter is used to form a special buried layer as a step toward silicon devices.

Synthesis and single crystal growth of indium phosphide in a one-step in-situ process at high ambient pressures is discussed. Analysis of heat transfer by convection, conduction, and radiation in a closed pressure vessel is given.

(Continued on Reverse)

20. DISTRIBUTION/AVAILABILITY OF ABSTRACT	21. ABSTRACT SECURITY CLASSIFICATION	
☐ UNCLASSIFIED/UNLIMITED ☒ SAME AS RPT ☐ DTIC USERS	UNCLASSIFIED	
22a. NAME OF RESPONSIBLE INDIVIDUAL Carl Pitha	22b. TELEPHONE (Include Area Code) (617) 377-3488	22c. OFFICE SYMBOL RADC (ESO)

Block 17 Cont:

20 12
20 14

Block 19 Cont:

A set of source modules and NOS procedures have been prepared to permit easy access to a 3-dimensional, non-isotrophic ray-tracing program (the Jones - Stephenson program). This "system" is designed to be run on a CDC CYBER computer system or equivalent using the NOS operating system.

TABLE OF CONTENTS

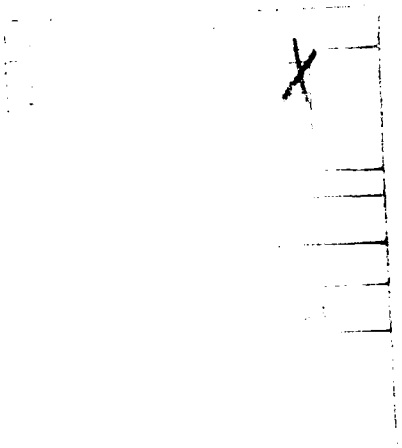

A-1

PREFACE

This report is composed of sections. It provides a summary of work accomplished under this contract in several diverse areas of optical transmission, materials and processing. The areas include:

I. Materials evaluation techniques under the general heading of electron microscopy. This includes the following methods of analyses: transmission electron microscopy, scanning electron microscopy, electron beam channeling, electron diffraction, and energy dispersive X-ray analysis.

II. A description is given of the experimental program on the synthesis, characterization, and single crystal growth of indium phosphide. The work is directed toward developing a single step, two phase process for the synthesis and single crystal growth of this material. A detailed description of the high pressure system is given together with data on the electrical characteristics and impurity levels of the synthesized material. Further discussion is given on the temperature-pressure profile and the effect of water cooled thermal baffling on the temperature profile.

III. Device processing techniques covering the use of an ultra high vacuum deposition system for evaporating a dielectric layer of silicon monoxide. This section also includes a discussion on the use of an ion beam implanter for forming special buried layers on silicon devices. The extreme usefulness of a residual gas analyzer to determine gas species within the vacuum chamber is shown.

I. MATERIALS EVALUATION TECHNIQUES

J. Comer

I. Introduction

Consultation for the past year has dealt primarily with the use of electron microscopy as a tool for identifying and evaluating materials used by the Air Force in electronic devices or in communication systems. Under the general heading of electron microscopy in this report are included the following electron optical methods of analysis: 1) transmission electron microscopy; 2) scanning electron microscopy; electron beam channeling; 3) electron diffraction; and 4) energy dispersive X-ray analysis. Used singularly or in combinations, the above techniques are used to identify bulk materials as well as very thin films and impurities within these materials. The crystalligraphic orientation can be determined and the physical make up, such as grain size and morphology, can be observed. The defects in single crystals, distributions, stocking faults and twins, can be detected and characterized. The JEM 100 C X/ASID electron microscope in these laboratories can perform all of these methods of analysis.

During the past year it was shown how these techniques could be applied to the study of the growth of thin epitaxial fibers on substrates. One example is VPE deposits on an IGaAs substrate. Work was also done on ion implanted silicon to determine the depth and nature of the implanted region. However, the most extensive use of the electron microscope was in the study of the nature of the PtSi films, formed on heating evaporated platinum films on silicon, which are used on Schottky diodes. Some details of this study will be given.

II. Platinum Silicide Formation on Silicon

1. Experimental Procedures

As part of a program to determine the best parameters for making Schottky devices using PtSi films, samples were obtained which had been completely characterized with regard to electrical performance. All films had been prepared in the same way, by evaporating platinum onto single crystal silicon at 350°C and then annealing in situ for 2 hours at 350°C. The parameter which was changed was the thickness of the platinum film, which varied from 5Å to 200Å in thickness.

2. Composition of The Film

The specimens were etched from the uncoated surface in 7:1 HNO_3-HF until a small hole was formed in the silicon. After washing the specimen to remove the acid, it was placed in a tilting specimen holder and examined by transmission electron microscopy. Over the hole through the silicon could be seen a continuous film which yielded a diffraction pattern which was usually different from that obtained with the beam through the thin region of silicon at the edge of the hole. The method is illustrated in Figure 1. Under (a) is seen the silicon substrate with the PtSi film formed by heating the platinum film to 350°C. After etching a small hole through the silicon (b), a film is observed over the hole. When the beam is placed in position A the selected area diffraction pattern shows the presence of the silicon substrate and a highly oriented film of PtSi. Sometimes a weak (111) reflection from unreacted platinum is also found. But when the electron beam is at position B, over the hole, there is

only a strong diffraction pattern from unreacted platinum and usually a pattern from polycrystalline Pt_2Si. Typical results for a 50Å thick platinum film are shown in Figure 2. Figures 2a and 2b are the electron micrograph and selected area diffraction pattern formed with the beam through the silicon as at A in Figure 1b. Figure 2c and 2d are electron micrograph and selected area diffraction patterns of the fibers only as seen with the electron beam at position B of Figure 1b. In Figure 2d the diffraction pattern from the residual film shows both Pt_2Si and Pt. Obviously, when the acid etches through the silicon the PtSi is removed. It is speculated that either the PtSi breaks up because of some solubility in the acid, or because some acid-soluble component in the grain boundaries, such as amorphous silicon, is dissolved. From the examination of shadow cast specimens and sterographic pairs of micrographics, it was determined that the residual film lies at the interface between the silicon and PtSi. It must be assumed that there is some porosity in this interface film which allows the acid to penetrate the PtSi film. In areas outside of the hole as at A in Figure 1b, the PtSi is protected by the silicon layer underneath and a layer of paraffin at the top, applied before thinning and removed before examining the specimen. In forming the diffraction pattern with the beam through the silicon the strong reflections from PtSi mask the Pt_2Si pattern, and only the strong (111) reflection from platinum can sometimes be seen.

3. Orientation and Lattice Size Changes

The sections of diffraction patterns seen in Figure 3 are from PtSi film formed from 10Å and 200Å in thick platinum films. In Figure 3a the thinner film shows only a strong 002 reflection of PtSi outside the 220 spot of silicon. This is consistent with the following epitaxial relationship of:

PtSi to silicon: $(1\bar{1}0)$ PtSi ll(001)Si
$[001]$ PtSi ll$[\bar{1}10]$Si
$[110]$ PtSi ll$[1\bar{1}0]$Si

In (b) the arc outside the 002 reflection is the 301 of PtSi, consistent with a second epitaxial relationship:

$(1\bar{2}1)$ PtSi ll(001)Si
$[30\bar{1}]$ PtSi ll$[1\bar{1}0]$Si
$[10\bar{1}]$ PtSi ll$[110]$Si

It has been observed in these studies that the first of these orientations prevails in the fibers formed from platinum of 10-20Å thickness but that increasing amounts of the second orientation are found as the film thickness increases. In measuring the actual d-values using selected area diffraction patterns from many specimens of different thickness, some were found to vary with film thickness. In Table 1 the 002 was observed to decrease with decreasing film thickness whereas the 220 was found to increase. The 301 showed no appreciable change. Such changes are not uncommon in very thin epitaxial fibers because of stress.

TABLE 1

COMPARISON OF d-VALUES FOR PtSi FIBERS OF DIFFERENT THICKNESSES

Film No.	Thickness of Pt	PtSi Reflections 002	301	220
CLD 217	200Å	1.796A	1.731A	2.034Å
CLD 219	100	1.795	1.730	2.039
LSD 124	40	1.779	1.725	2.060
CLD 207	20	1.782	1.729	2.059
CLD 205A	10	1.782	1.734	2.050
CLD 200A	10	1.786	Not Measureable	2.048
Bulk Specimen (ASTM)		1.804	1.737	2.037

4. Grain Size and Film Thickness

Individual grains in the epitaxial films were difficult to see in the very thin films, 50Å or less, and are best imaged by tilting the specimen to obtain a strong 220 silicon spot. Under these conditions the grains show Moire fringes as seen in Figure 2a and 2c. Although exact dimensions are not necessarily given by the fringe patterns, it was evident that the largest size grain in films found from 10Å of platinum are about 200Å in diameter and reach as high as 800Å in PtSi films formed from 200Å thick platinum.

III Summary

It was shown how electron optical techniques could be used to identify and characterize electronic device and electro-optical materials. In particular the formation of PtSi on silicon in the very thin film range (5-200Å) was studied. From these, grain size and

lattice parameters were determined as a function of fiber thickness. An interesting new finding in this study was the presence of a layer between the PtSi and silicon in which unreacted platinum and Pt_2Si are found.

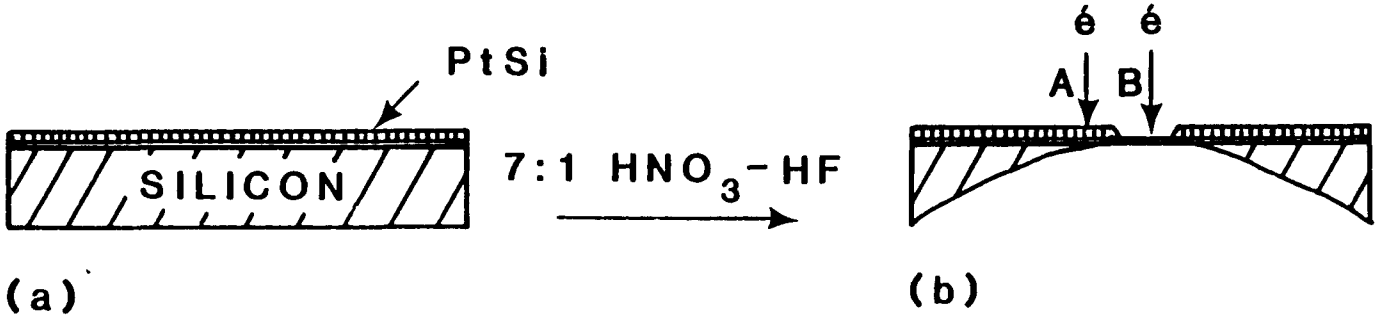

SILICON SUBSTRATE WITH LAYER

Figure 1

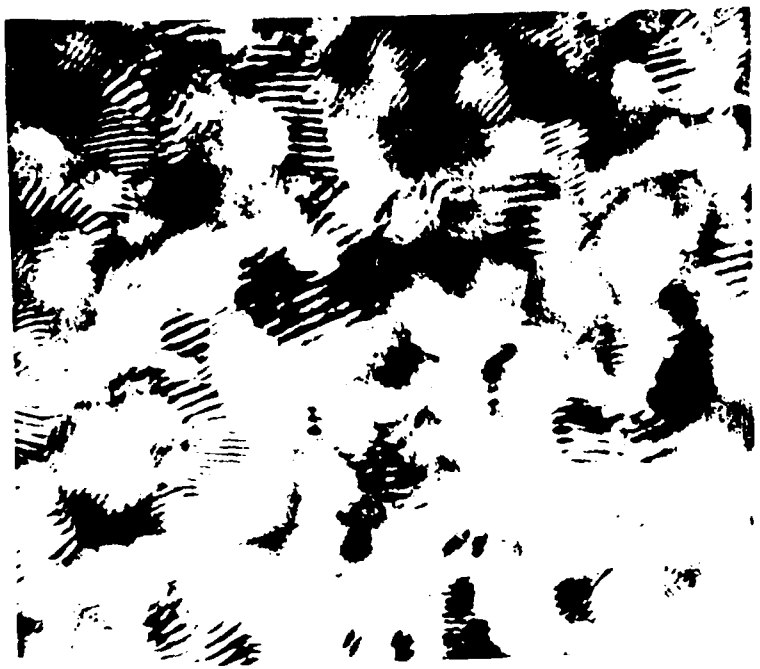

(a) x500,000

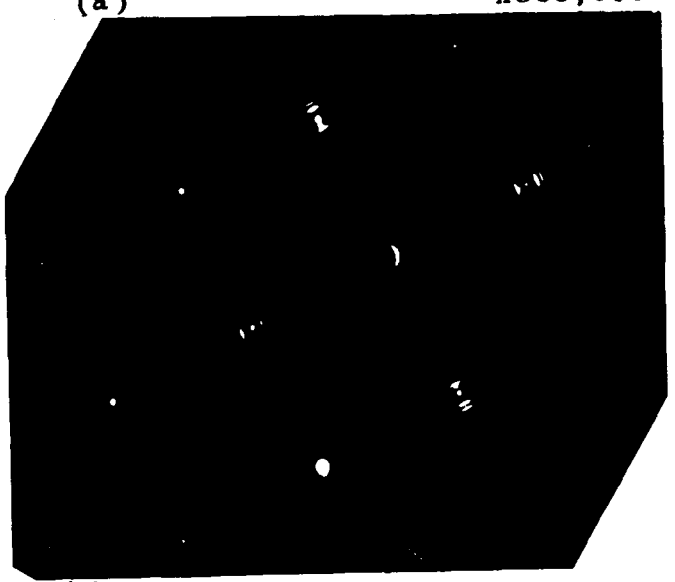

(b)

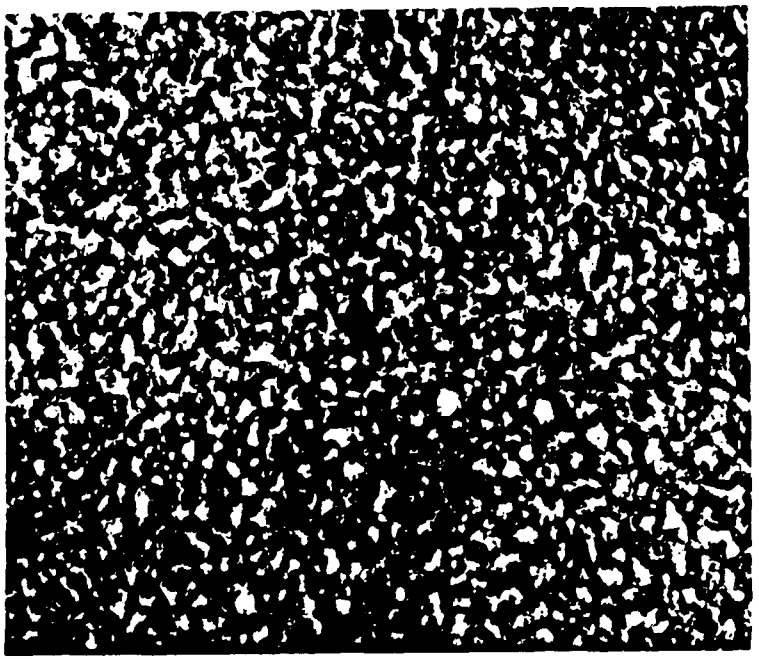

(c) x150,000x

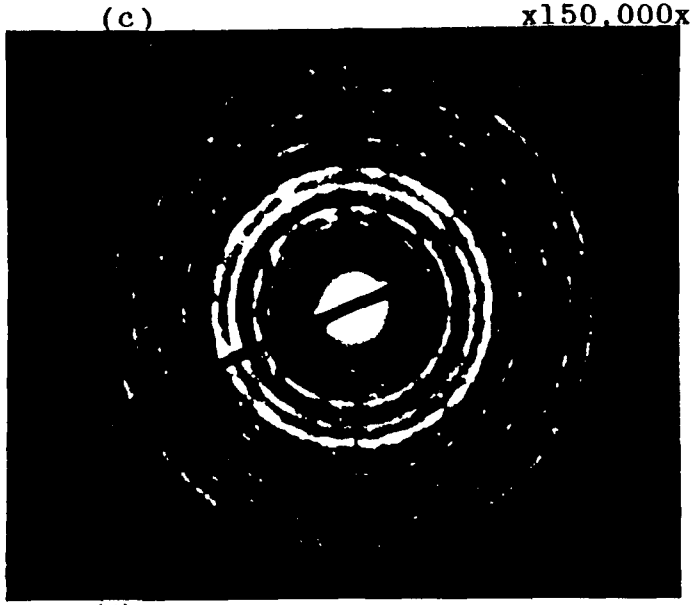

(d)

FIGURE 2 - PLATINUM SILICIDE FILM COMPARISON. COMPARISON OF THE PtSi FILM FORMED OVER SILICON IN a AND b, AND THE RESIDUAL Pt Si/Pt FILM (c AND d) LEFT AFTER ETCHING A HOLE THROUGH THE SILICON

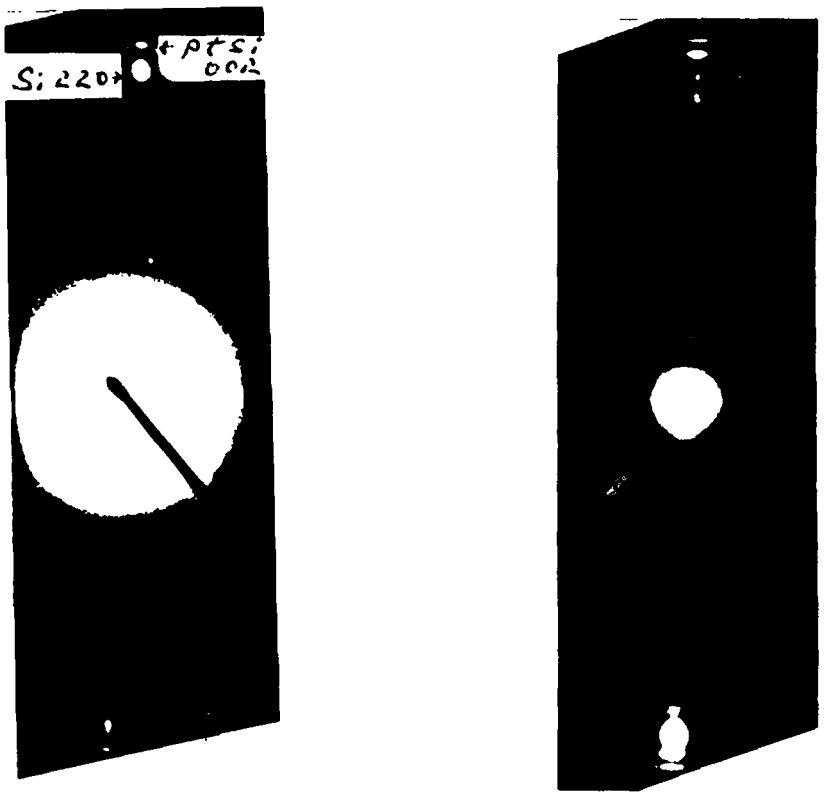

(a) (b)

FIGURE 3

IN (a) A STRONG 002 REFLECTION APPEARS ABOVE THE 220 SILICON SPOT FOR PtSi FORMED FROM A 10A Pt FILM. IN (b), PtSi FORMED FROM A 200Å THICK Pt FILM, A STRONG 301 REFLECTION APPEARS ABOVE THE 002 REFLECTION, INDICATIVE OF A SECOND STRONG EPITAXIAL RELATIONSHIP OF PtSi TO SILICON.

II. SYNTHESIS, CHARACTERIZATION AND GROWTH OF INDIUM PHOSPHIDE

Robert C. Marshall

The importance of indium phosphide is demonstrated by its potential for microwave and opto-electronic devices. One of the major reasons for the current interest in opto-electronic devices (ternary or quarternary thin films i.e. GaIAsP on InP substrates) is the dramatic improvement in optical fibers particularly in the 1.1-1.6 micrometer wavelength region. These thin-film devices require InP substrate material of the highest purity with controlled impurity levels. It is most important that the quality and availability of the substrate material be improved. It is difficult to see how the demand for InP can expand to any great extent until the cost of producing the material is substantially reduced.

The objective of this effort is divided into two phases. First, the controlled syntheses of indium phosphide with the highest purity by an intensive research effort to purify each element of the compound to obtain the highest purity possible. Vacuum baking of the indium (10^{-8} - 10^{-9}torr) at select temperature over various periods of time has been extremely successful. Double vacuum baking, hydrogen streaming and the use of various boat materials such as using quartz and pyrolytic boron boats interchangeably with boron oxide and aluminum oxide tubes to help reduce silicon contamination from the SiO have all been tried. The purification of elemental phosphorus is a very difficult problem to solve. We are presently developing and fabricating apparatus to purify the phosphorus by passing phosphorus gas through molten lead. The lead to serve as a getter for impurities

in the phosphorus. These experiments are only in the early stages.

Experimentation

A sketch of the high pressure vessel is shown in Figure 1. The various parts of the systems are indicated by the letters. A shows the end of the two section heater for the indium zone; B shows the water-cooled thermal baffle; C is the heater for the phosphorus zone; D is the pressure gauge which shows the internal pressure of the vessel during the experiment; E shows one of eight thermalcouples. Two are in each section of the indium zone, two in the phosphorus zone with one of these attached to the phosphorus end of the ampoule. This T.C. indicates the exact temperature of the phosphorus during the experiment. Two thermacouple are attached to the indium end of the ampoule, one at the front-of-the-boat. It is desirable to have a steep thermal gradient from the front end of the boat which contains the InP seed and the back of the boat. F1, F2 and F3 show the power leads to the two-section indium heater. F4 is one of the electrodes to the phosphorus heater.

A typical layout of the furnace system showing ampoule, plug, boat, phosphorus, water cooled baffle, heat pipe and temperature profile is shown in Figure 2. The temperature of the front-of-boat and back-of-boat is such as to maintain a temperature differential so that during the synthesis process, the boat front (end nearest the phosphorus zone) is always cooler than the other end. This is essential when seeding at the boat front.

Figure 3 shows the indium temperature profile, furnace vessel pressure and phosphorus temperature over the complete synthesis cycle. The temperature of the indium zone is brought to 800^{o}C and left for 16

hours (overnight). It is then raised to 1090°C for a period of several hours while the phosphorus temperature and furnace overpressure are gradually increased. When the phosphorus zone has reached 540°C the furnace overpressure has gradually been raised to 350-400 PSI. After all the temperatures and pressure have been stabilized, a soak period of several hours is maintained. After this soak period, the temperature in the indium zone is gradually reduced at a rate of 18°C per hour while maintaining a temperature differential between the front and back of the boat. This gradient is accomplished by controlled decreasing of the indium heater (the section closer to the phosphorus zone). While the total length of the experiments vary, the average is around 28-30 hours.

Several high pressure synthesis experiments have been accomplished. Two of these experiments resulted in ampoule explosions when we were unable to control the temperature in the phosphorus zone. Once the temperature starts to rise, the phosphorus pressure increases, travels by convection to the indium zone, is heated to 1100° C, then travels back to the phosphorus zone, heating the phosphorus more, thereby increasing the gas pressure. This convective cycling continues until the pressure in the ampoule exceeds the ambient overpressure (500 PSIG is maximum furnace capability) and the ampoule explodes. Control of the phosphorus temperature is therefore essential. The addition of the potassium filled heat pipe and the two-turn water cooled coil help permit independent temperature control of the phosphorus zone. Some adjustment of the temperature in that zone can be accomplished by varying the flow rate of the cooling water. Analysis of the heating and cooling rates is being continued to determine optimum conditions.

The top surfaces and cross-sectional slices of indium phosphide ingot HP-2 are shown in Figure 4. Van de Pauw measurements were made on grains selected from the polycrystalline charge and are shown in Table 1. These values are consistent with those achieved with standard low pressure Bridgman synthesis.

Polycrystalline wafers cut from the first-to-freeze portion of the ingot were analyzed by two techniques to identify, quantitavely, the chemical nature of the ionized impurities shown in the Hall measurements (Table 1). Emission spectroscopy results were inconclusive since many impurities were below the detection limit. Atomic absorption measurements are shown in Table 2. Both of these techniques were unable to detect sulphur which is the dominant impurity in high mobility indium phosphide.

Vacuum baking of the indium has reduced the concentration of silicon and sulphur below 1×10^{15}. Purification studies are being initiated in an attempt to improve the quality of the starting phosphorus.

Figure 5 shows an indium phosphide ingot cut in half. This ingot was synthesized under asymetric thermal conditions at the boat. Note the large crystals at the top, bottom and ends of the ingot. After etching, the interior showed small crystallites and vacant areas where the unreacted indium was etched away. The crystal froze from the top and bottom trapping elemental indium in the center. The top surface of the ingot can be seen in Figure 6. As the ingot continued to freeze, compression of the molten indium forced bubbles to the surface of the indium phosphide still semi-molten. Note these projections on the surface of the ingot. The large single crystal shiny surface on the top of the ingot extends well below the surface. The cooling

cycle of the newly formed indium phosphide should be sufficient to allow the interior of the ingot to cool before the outside areas are frozen. In this experiment, the back-of-the-boat temperature fell too rapidly.

Since our objective of these experiments was to combine the synthesis and single crystal growth into a one-step process, a gallium phosphide seed (essentially the same lattice constant as InP) was inserted at one end of the boat. A gallium phosphide seed was used because the seed was inserted in the boat prior to the indium vacuum baking purification process at 800°C. Figure 7 shows the surface of the indium phosphide ingot with the seed end clearly visible. Note the propogation of the crystals from the seed end. While the ingot was not single crystal, it showed promise that further work with this technique could be quite rewarding.

A technique has been devised whereby the indium in the boat could be vacuum baked and an indium phosphide seed inserted after the baking. After the seed is inserted in the boat, the indium is remelted under vacuum but only at a temperature of 200°C. This does not cause the phosphorus to outgas from the indium phosphide seed.

Consultation was also provided in the design of a high pressure crystal growth furnace system with magnetic melt stabilization. As has been discussed in earlier quarterly reports, the synthesis and single crystal growth of indium phosphide should ideally be accomplished in the same furnace system. Our design is being directed toward a stacked two-chamber configuration connected by a large opening (6") gate value. Both chambers would have a pressure capability from 10^{-5} torr to 750 PSIG. The lower chamber encompassing the R.F. Coil, crucible and indium and phosphorus charge would be

surrounded by a large magnet to stabilize the melt during Czoehralski or Kyropoulos single crystal growth. A more detailed description will be given in the next report on this contract.

I am also designing a new one-step synthesis-crystal growth technique which will eliminate the synthesis process as a separate step. At present I am analyzing the various sequential steps of the process as to material densities, melting points, impurities, thermal stepping, phosphorus pressures ambient pressures required and heats-of formation. The original design concept is completed. Further technical discussions will be given in the next report.

In consulting with the scientist at ESM, we have discussed the technical aspects of many problems associated with crystal synthesis, crystal growth, temperature control and stability at high pressure, thermal work profiles, possible new designs of crystal synthesis and single crystal growth systems, vacuum baking as a material purification technique and many other aspects of the electronic and optical materials problems. These discussions often result in developing new experimental techniques or approaches that have direct impact on the results of our experimental research. Further discussions and experiments will continue during the next reporting period.

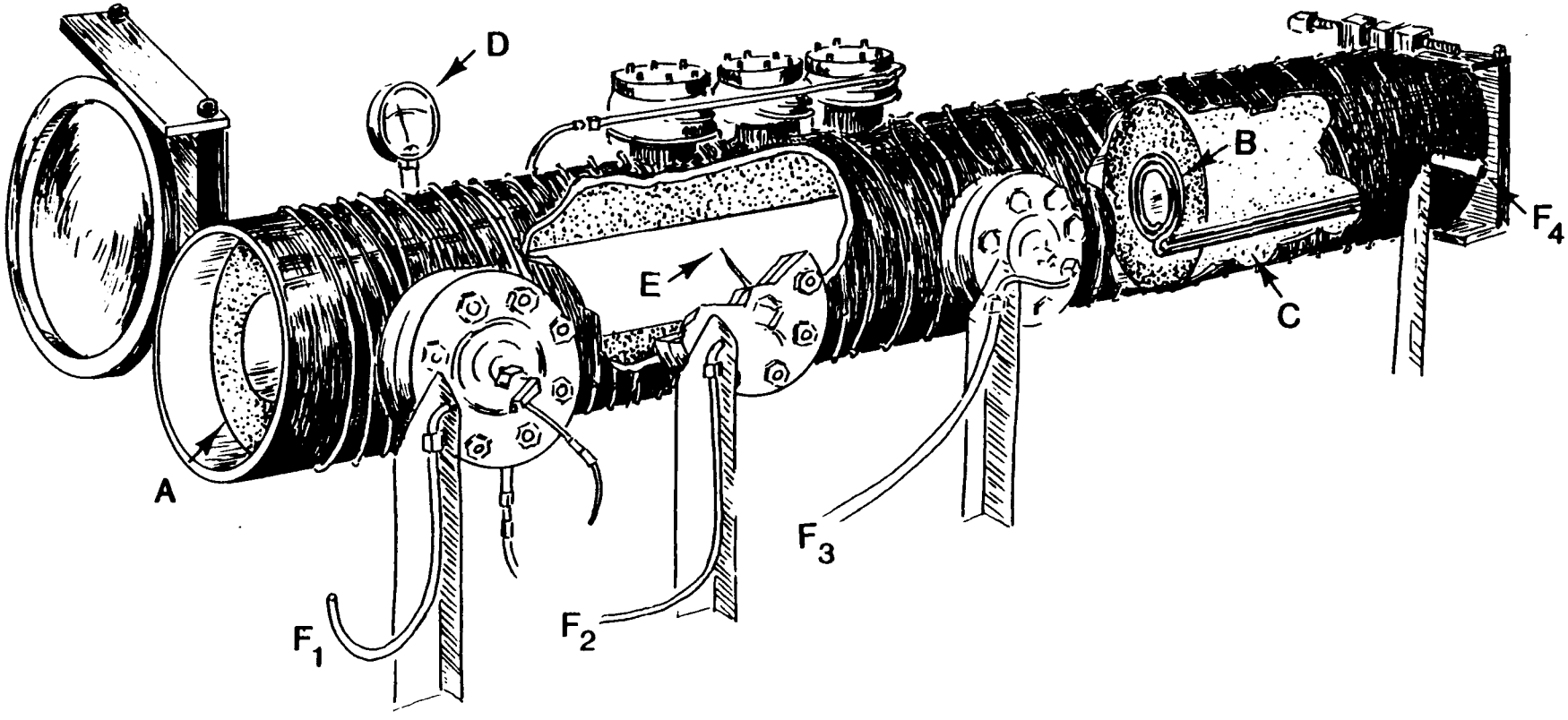

FIG 1

SKETCH OF HIGH PRESSURE FURNACE SYSTEM

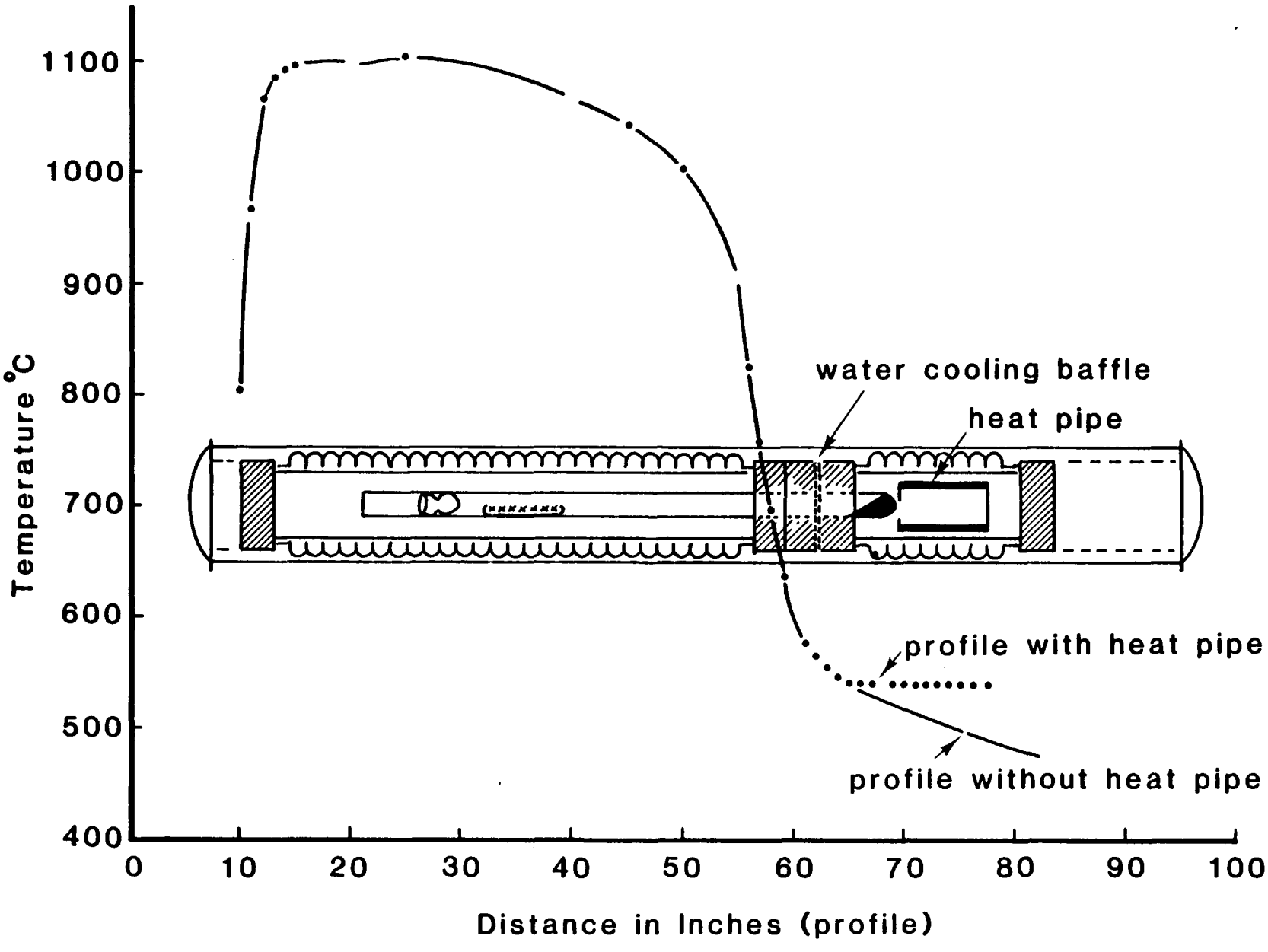

FIG 2

THERMAL PROFILE WITH AMPOULE, BOAT, HEAT PIPE AND HEATERS

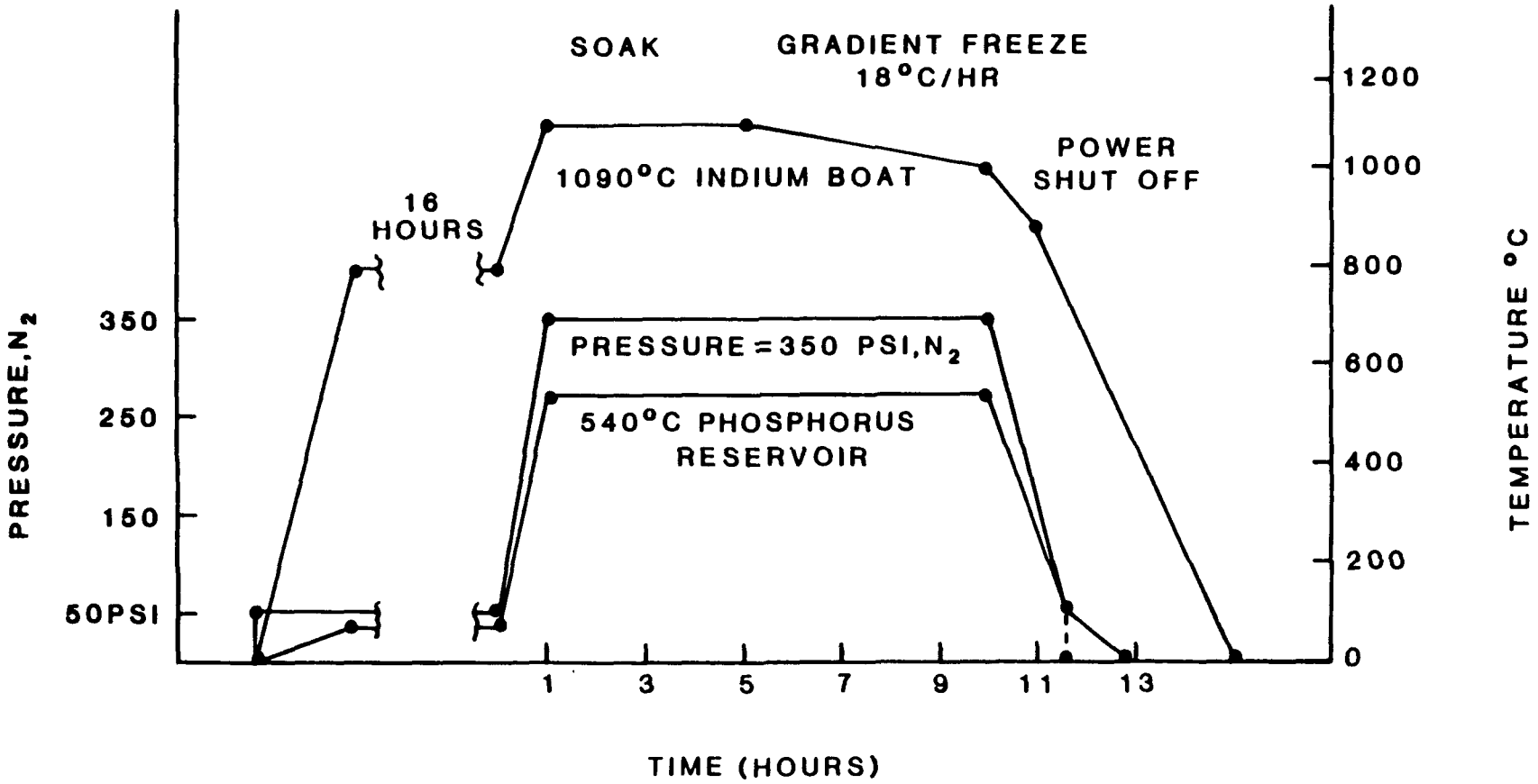

FIG 3

TEMPERATURE-PRESSURE TIME CYCLE

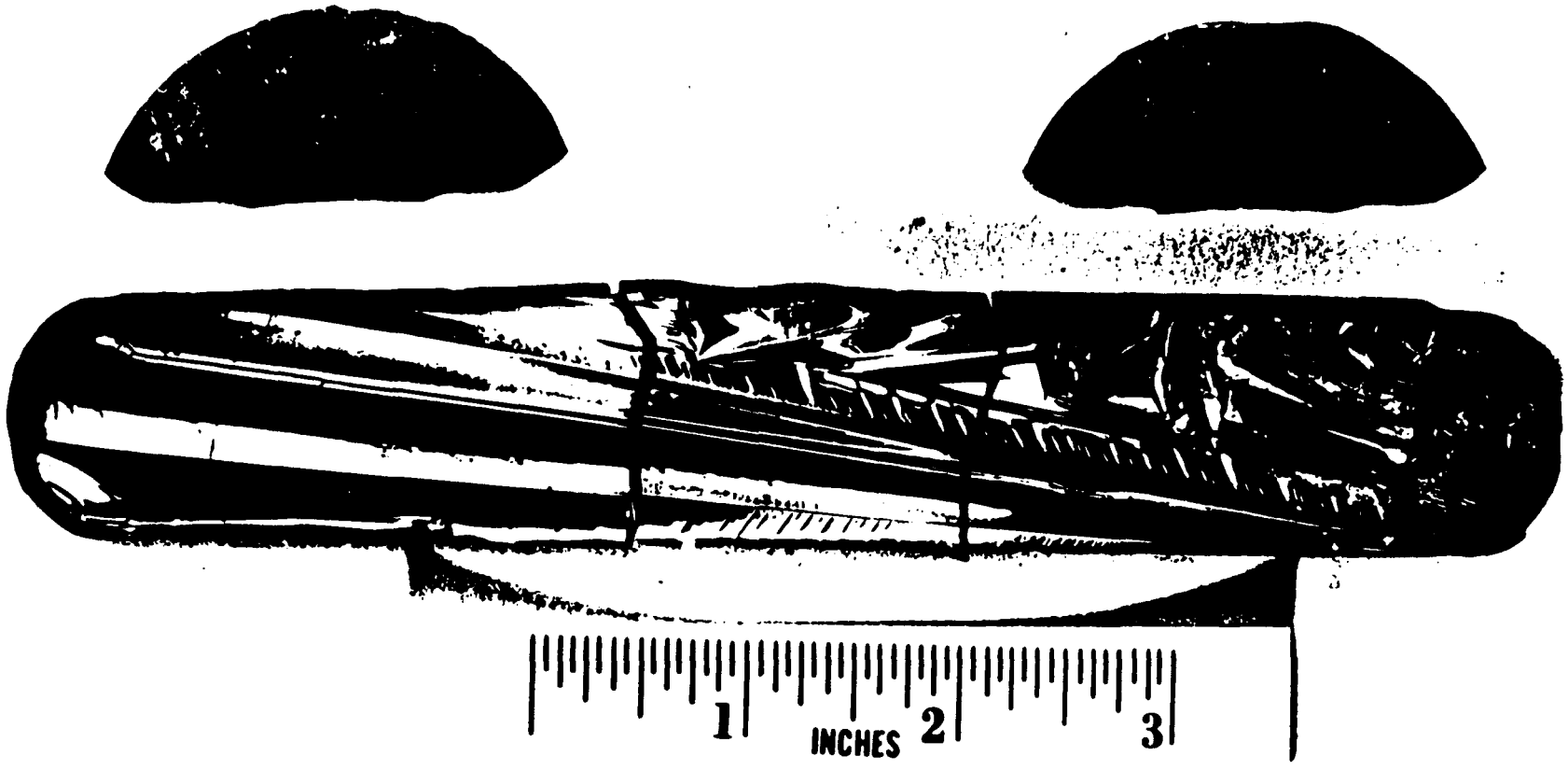

HP-2

FIG4

INDIUM PHOSPHIDE INGOT AND ETCHED SLICES

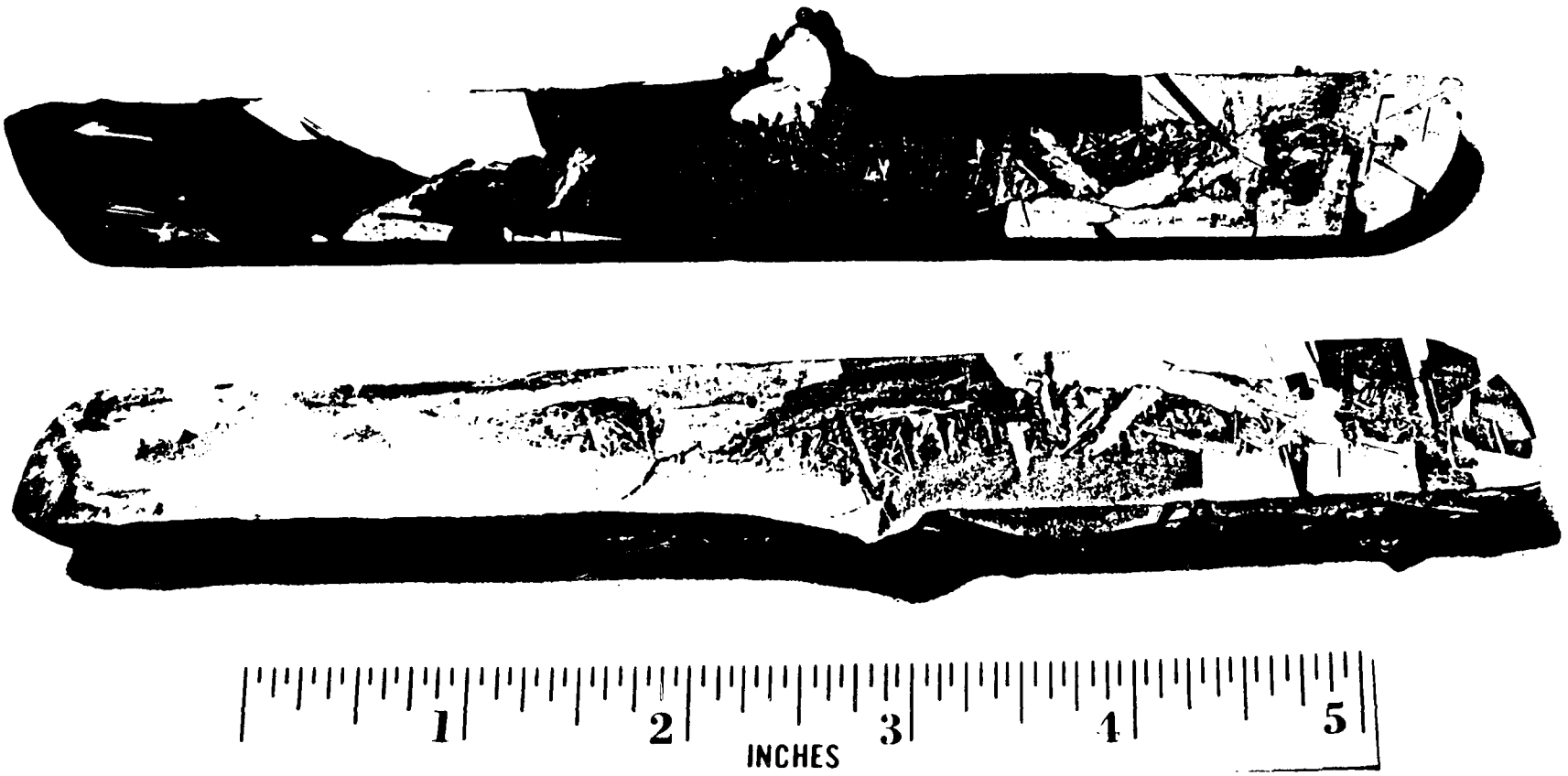

FIG5

SECTIONED INDIUM PHOSPHIDE INGOT


1
2
INCHES
3
4
5
TOP SURFACE OF INGOT

FIG7

TOP SURFACE OF SEEDED INGOT

SAMPLE NUMBER	μ 77K $CM^2/V-SEC$	μ 300K $CM^2/V-SEC$	n x 10^{15}
HP-1	29,500	4974	2.4
HP-2	35,100	4428	4.1
HP-5	21,500	3355	6.0
HP-6	32,900	4154	4.3

TABLE 1

MOBILITY MEASUREMENTS

	Si	Fe	Al	Cu	Zn
HP-5	ND	11	5	4	<1
HP-6	ND	9	7	4	<1
HP-7	ND	9	7	3	<1

AAS VALUES ARE IN PARTS PER MILLION

TABLE2

IMPURITY CONTRACTIONS

III. DEVICE PROCESSING TECHNIQUES

J. Bloom

Consultation to ESE scientists was primarily in three areas. These areas were: an ultra high vacuum deposition system for preparing silicides having infrared sensitivity; a vacuum deposition system for evaporating a dielectric layer of silicon monoxide (SiO); and, an ion beam implanter for forming special buried layers on silicon devices. Other consultations on general vacuum problems were relatively minor in comparison to the major effort on the above three systems.

1. Ultra High Vacuum Deposition System for Select Silicides

Examination of the photograph (Figure 1) shows the control equipment in the rack. From the bottom to the top of the rack, 1 is the control and power supply of the electron beam evaporator; 2 is the ion pump control and power supply; 3 is the control for the sublimation pumps; 4 is the control for bake out of the bell jar, the ion pumps and the sorption pumps; 5 is the thermistor vacuum gauge for aid in roughing the bell jar system; 6 is an x-y plotter that is used with the residual gas analyzer; 7 is the thin film thickness monitor; 8 is the power supply used to heat the substrates (silicon wafers); 9 is the high vacuum gauge that controls a nude ion gauge tube mounted in the bell jar. To the right of the equipment rack is the ultra high vacuum system; 10 is the stainless steel bakeable bell jar. Not visible inside the bell jar are the deposition monitor sensor mounted on the shutter plate and the heated substrate holder

with a thermocouple for temperature control. The manual shutter is controlled by 14; 11 is the evaporation source, the crucible and magnet of the electron beam gun; 12 is the bakeable chamber containing the ion pump, the sublimation pump and the meisner trap; 13 are the sorption pumps A, B, and C; 14 is the roughing manifold; 15 is the mirror used for viewing the molten metal in the crucible. Behind the rack not shown is a port with the residual gas analyzer head connected to the system through an UHV bakeable value and the heating mantle on the head. The normal procedure for the formation of an infrared sensitive metal silicide Schottky diode has been standardized.

The bell jar is not opened until the sorption pumps are well chilled. As rapidly as possible the sample is placed on the substrate holder. After closing the bell jar the sorption pumps are used serially to lower the bell jar pressure to 10 milliTorr or less. The ion pump is turned on and then when the pump has "started", (can maintain the pressure without the sorption pumps), the main valve is closed. The ion pumps are baked out first, then the bell jar. The gas analyzer is activated and if the gas ambient is normal, the substrate heater is turned on. When the substrate holder thermocouple reaches the right temperature for the metal silicide being formed, the electron beam gun is turned on, the melt is outgassed and the shutter is opened to allow proper thickness of the metal to fall on the silicon surface. The shutter is closed and the sample is held at the proper temperature for a time determined by the metal used. The sample is allowed to cool and is removed when the next sample is loaded.

The residual gas analyzer is a very powerful diognostic instrument for this vacuum system. A new instrument dedicated to this system will be installed in the first quarter of the next fiscal year.

The usefulness of a residual gas analyzer can readily be illustrated by refering to the following plots of gas ambiant.

Graph 1 shows the gases present in a well processed UHV system. The large off-scale peak at mass 2 is due to hydrogen H_2. It can also be a fragment of water vapor mass 18 or any hydrocarbons present. The peak at mass 4 is due to Helium. Mass 12 is carbon from hydrocarbons or mass 28 carbon monoxide or mass 44 carbon dioxide. Mass 14 is a fragment of mass 28 due to nitrogen N_2. Mass 14 is a frament of nitrogen N or a fragment of methane (CH_4) CH_2. Mass 15 is also a fragment of methane. Mass 16 is methane or oxygen O. Methane can be made by the pumping action of the ion pump on hydrocarbons or by carbon dioxide and hydrogen. Mass 17 is a water fragment OH. Mass 18 is due to water vapor H_2O. Mass 20 is NE or HF, since HF is used to etch wafer it is no doubt one of the species present. Mass 32 is due to O_2.

Graph 2 is a bar graph showing at a gain of 33 times higher than the previous analog trace. Even at the higher gain one can see no trace of any species above mass 50 which shows no hydrocarbons from oils or solvents are present. The other peaks are all due to fragments. Graph 3 is a bar graph at the same gain as Figure 2.

Partial Pressures and Gas Composition Calculation

The quantitative characteristics of the RGA may be used for measurement of the absolute pressure of a component in a mixture of

gases (the "partial pressure") or the relative amount of each gas expressed as a percentage of the total.

The following symbols will be used:

PP = Partial pressure of a given substance "A" in a gas mixture - torr.

I = Current output of the RGA sensor, signal amplitude of a mass peak, "B" resulting from substance "A".

FF_{AB} = Fragmentation factor, fraction of total ions from substance "A" having mass "B".

FF_{N28} = Fragmentation factor for N_2^+ ions from nitrogen (typically .90 to .95 and often taken as 1.0).

TF = Transmission factor, the number of ions of mass "B" that pass through the analyzer, relative to ions of mass 28. TF = (28/M) (nominal).

DF = Detection factor, the relative current per ion at mass "B" compared to nitrogen ions at mass 28. For the RGA with Faraday Cup, DF = 1. For the RGA with electron multiplier, DF = 1 when voltage is 2,000 volts.

S = Sensitivity for nitrogen, output current (at mass 28) per unit absolute pressure for pure nitrogen-amp/torr. For the RGA with electron multiplier, S varies widely depending on the operating voltage and condition of the multiplier. For a new sensor S = 1 at a voltage typically in the 1800-2000 range.

Then we can say, the partial pressure of substance "A" indicated by the amplitude (I) of signal at mass "B" is

$$PP = (I \times FF_{N2B})/(FF_{AB} \times XF \times TF \times DF \times S) \qquad (1)$$

This equation is quite general and holds true for all mass spectrometers.

The constants for these equations can be obtained from tables or, for best accuracy, measured for each instrument (instruments will

not be identical).

During the twelve months of this reporting period, this system has been redesigned and improved remarkably to the point that successful devices can be fabricated in this system as a result of change suggested by my consultation with ESE scientists.

2. The dielectric evaporation system has a conventional oil diffusion pump (1) (Figure 2) and a mechanical pump (2) to back it. The liquid nitrogen trap (2A) is used to pump water vapor rapidly when cycling the system. The power supply control panel (3) controls the current that heats the boat that contains silicon monoxide used as the dielectric layer. The manual values are controlled from a panel (4), 4a and 4b are inlet values panel (5) has mounted on it the vacuum thermocouple gauges. The thickness monitor (6) control works with the deposition thickness sensor (10). The boat not seen is held by the high current electrodes (7). The chimney (8) limits the spread of the evaporant to the substrate holder (9).

Samples have shown an exceptable low variation of thickness and the samples have been used to develop an etch for device manufacturing.

3. The ion implanter, in spite of its apparent complexity, is basically a high-current mass analyzer. Figure 3 shows the high voltage section which has two functions. One is to ionize the species to be implanted and the other is to accelerate (and focus) the ion to the desired energy. A heated tungsten filament is used as the electron source in the ionizer section. Figure 4 shows the magnet of the analyzer section on the left edge. The ions are bent

with the magnet and, depending on the M/e of the ion, it is bent with the magnet to hit an analyzing slit.

The beam is scanned in an XY direction to cover the wafer. Figure 5 shows an equipment rack. On the top shelf is a ramp generator used to drive the four power supplies in the scan mode. Built in the power supply is a power source used with manually set potentiometers to set the mass to be implanted by adjusting the strength of the magnetic field. Figure 6 shows most of the implanter vacuum system. The samples to be implanted are mounted in chamber A. This can be cooled by LN_2. B is the electromagnet used to bend the beam. C is a turbo molecular pump used to keep pressure low.

Ion implantation replaces the conventional doping method of diffusion. In semiconductor manufacturing, ion implantation is the direct injection of dopant atoms or molecules into semiconductor wafers. The injection is done while using a patterned mask on the wafer. The pattern is generated by photo lithography. This enables fabrication of precisely delineated regions of doped semiconductors. Ion implantation can provide accurate doping and control of the doping profile and junction depth within the semiconductor.

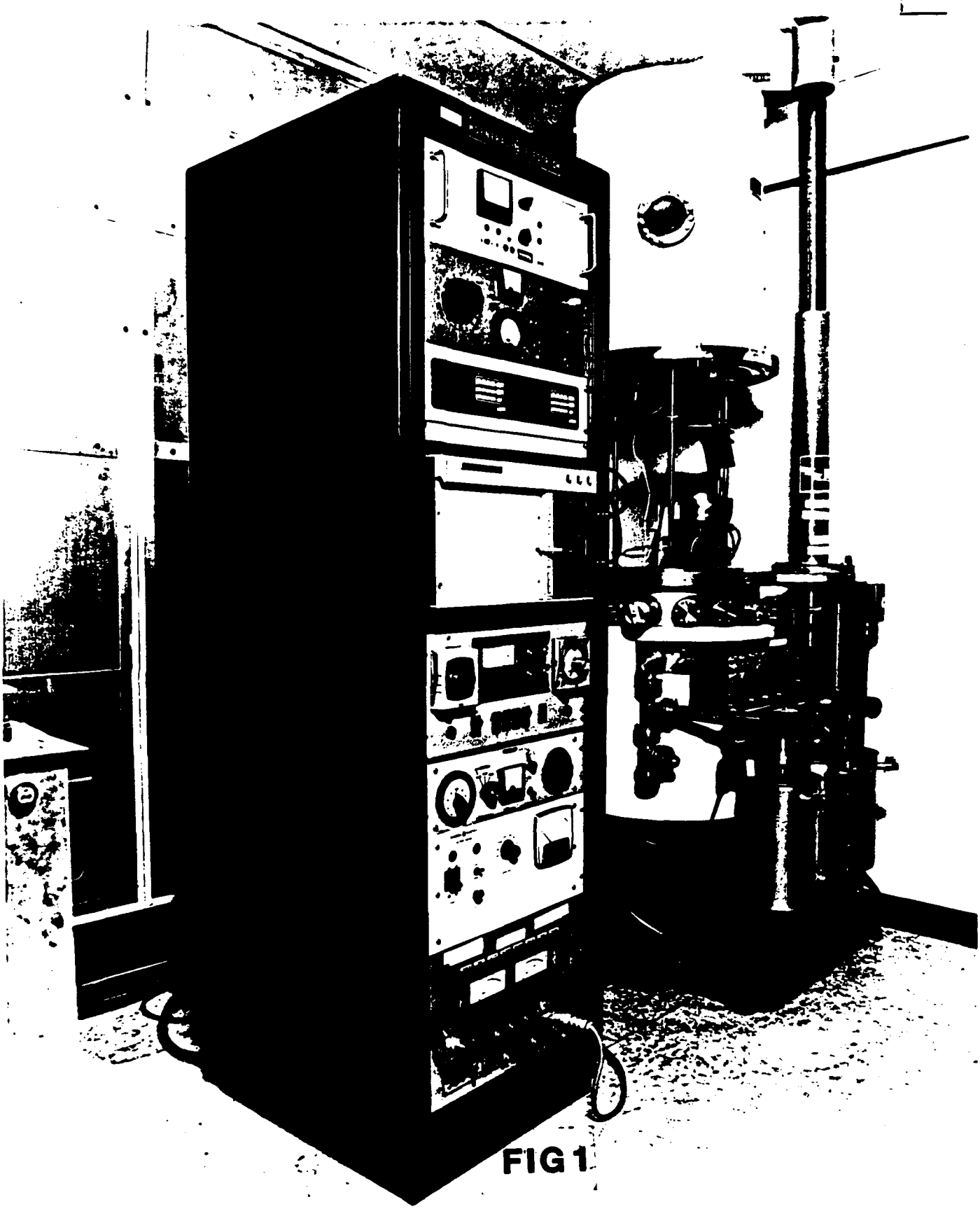

FIG 1

UHV CONTROL EQUIPMENT

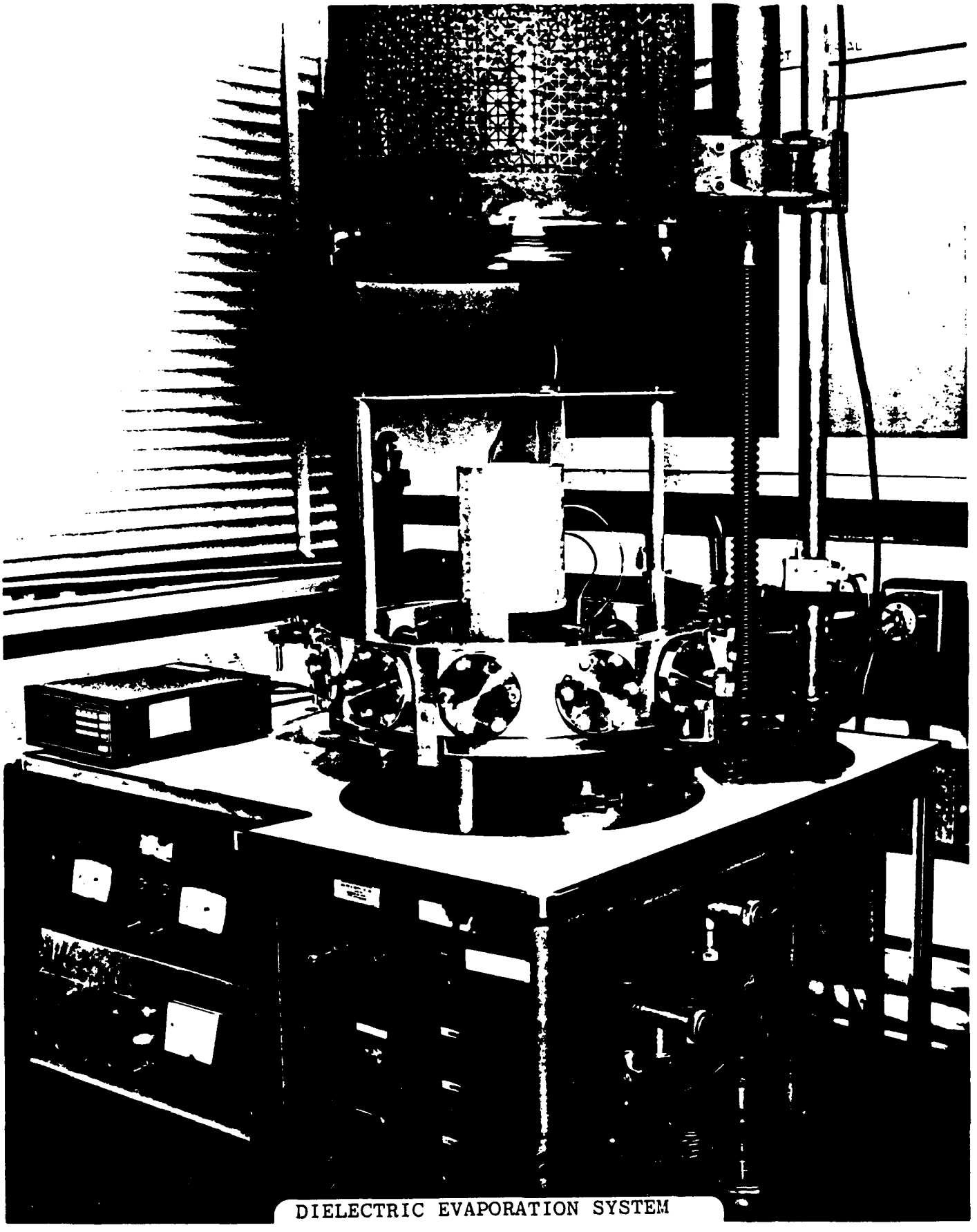

DIELECTRIC EVAPORATION SYSTEM

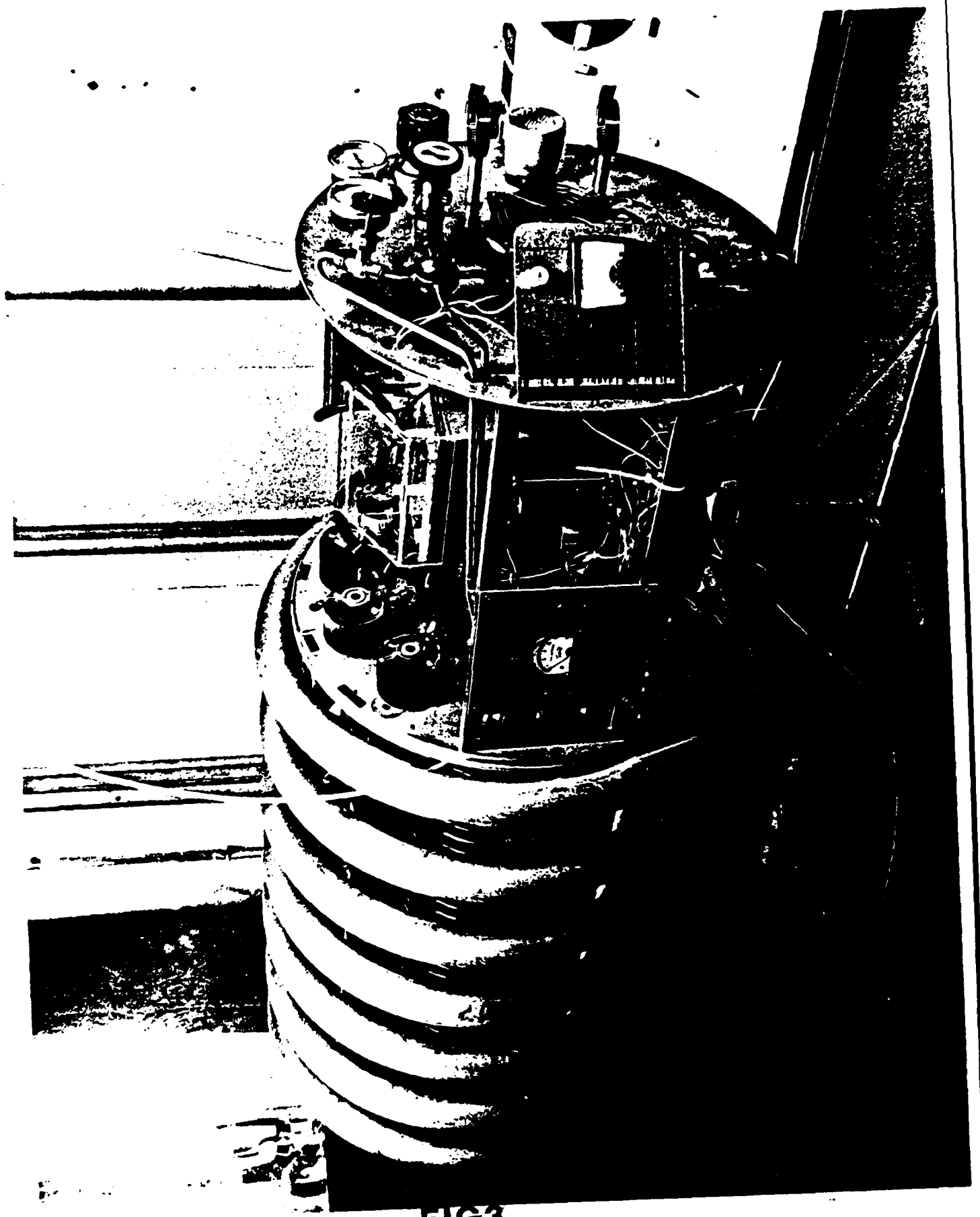

FIG3
ION IMPLANTER HIGH VOLTAGE SECTION

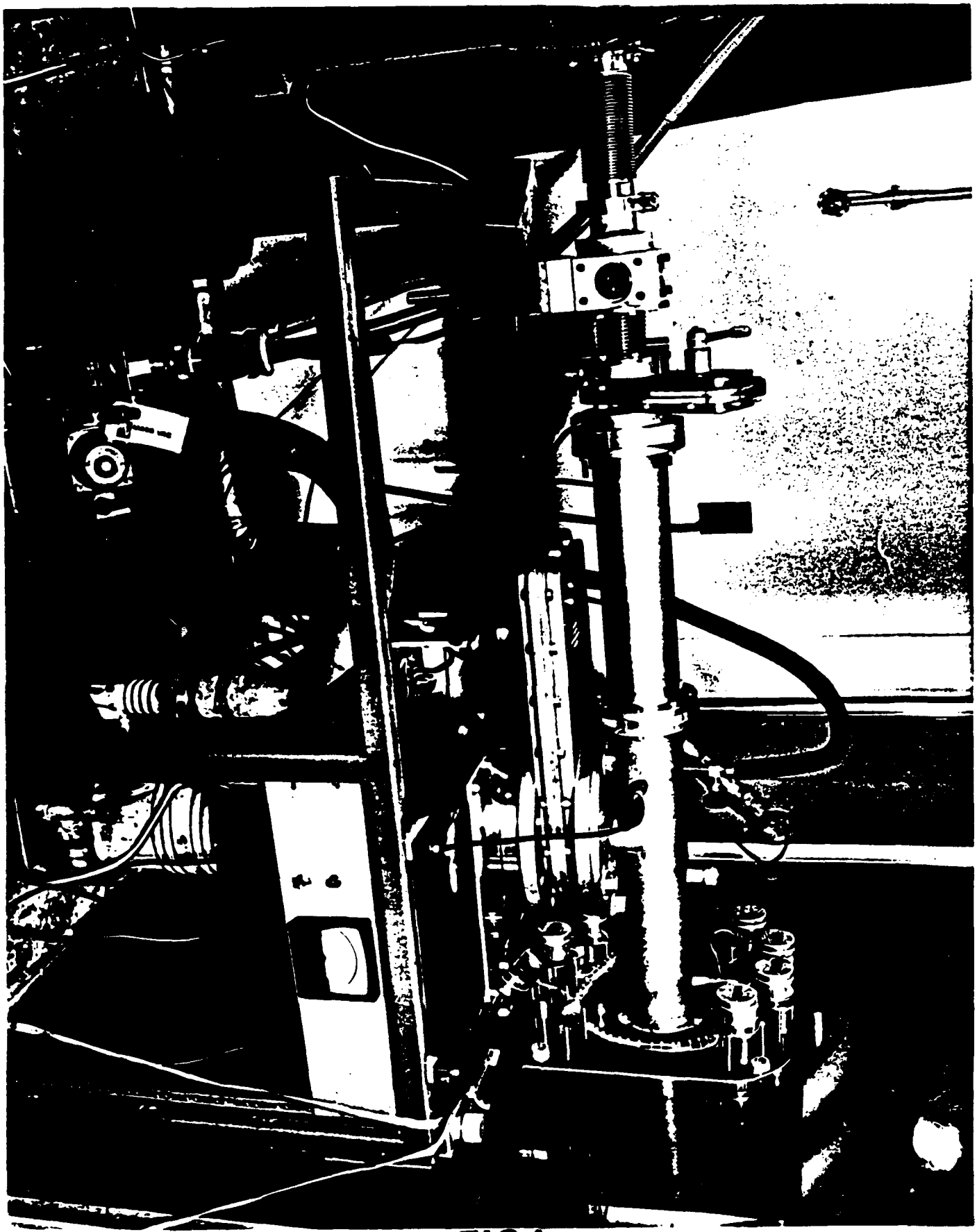

FIG4

MAGNET AND VACUUM PLUMBING

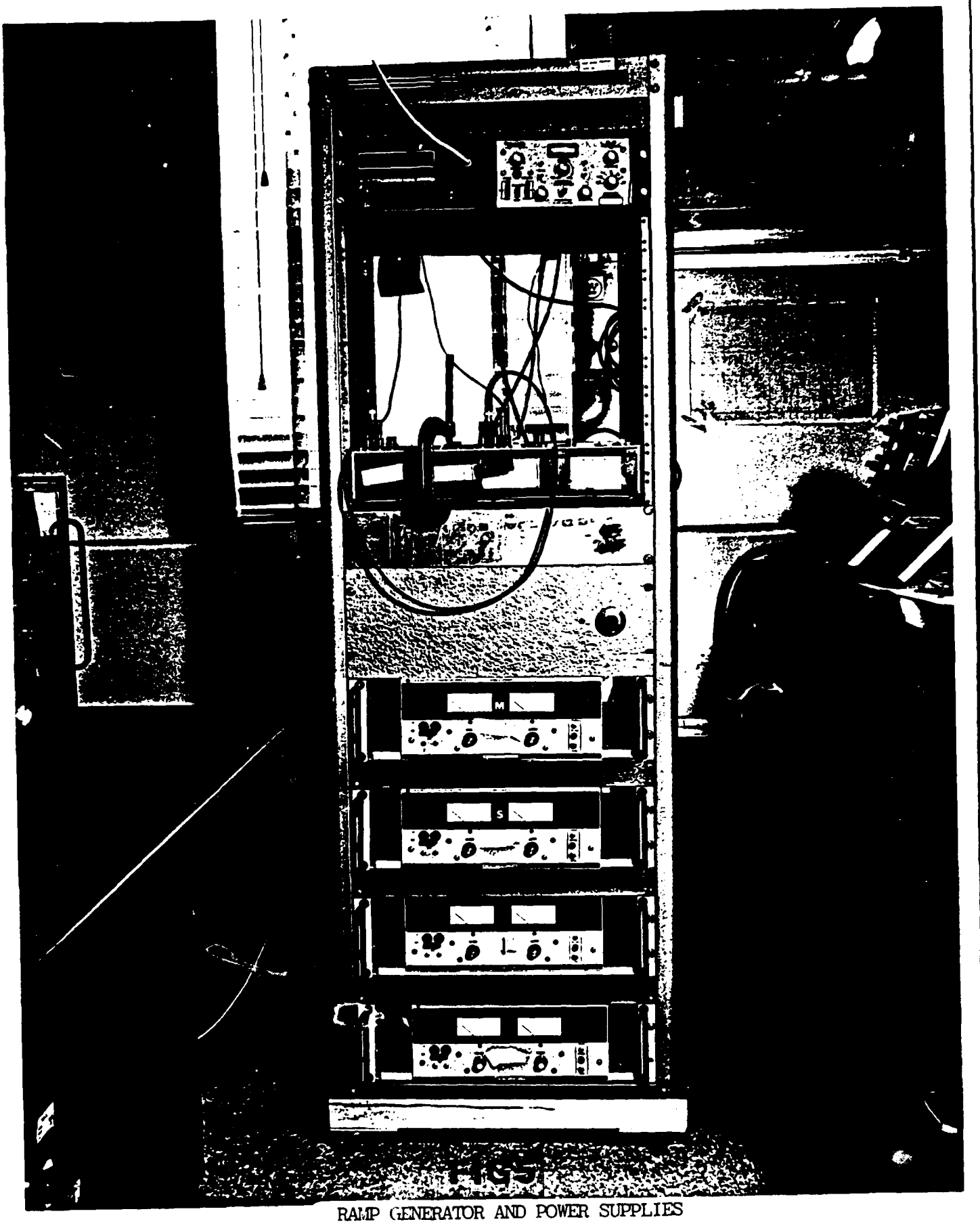

RAMP GENERATOR AND POWER SUPPLIES

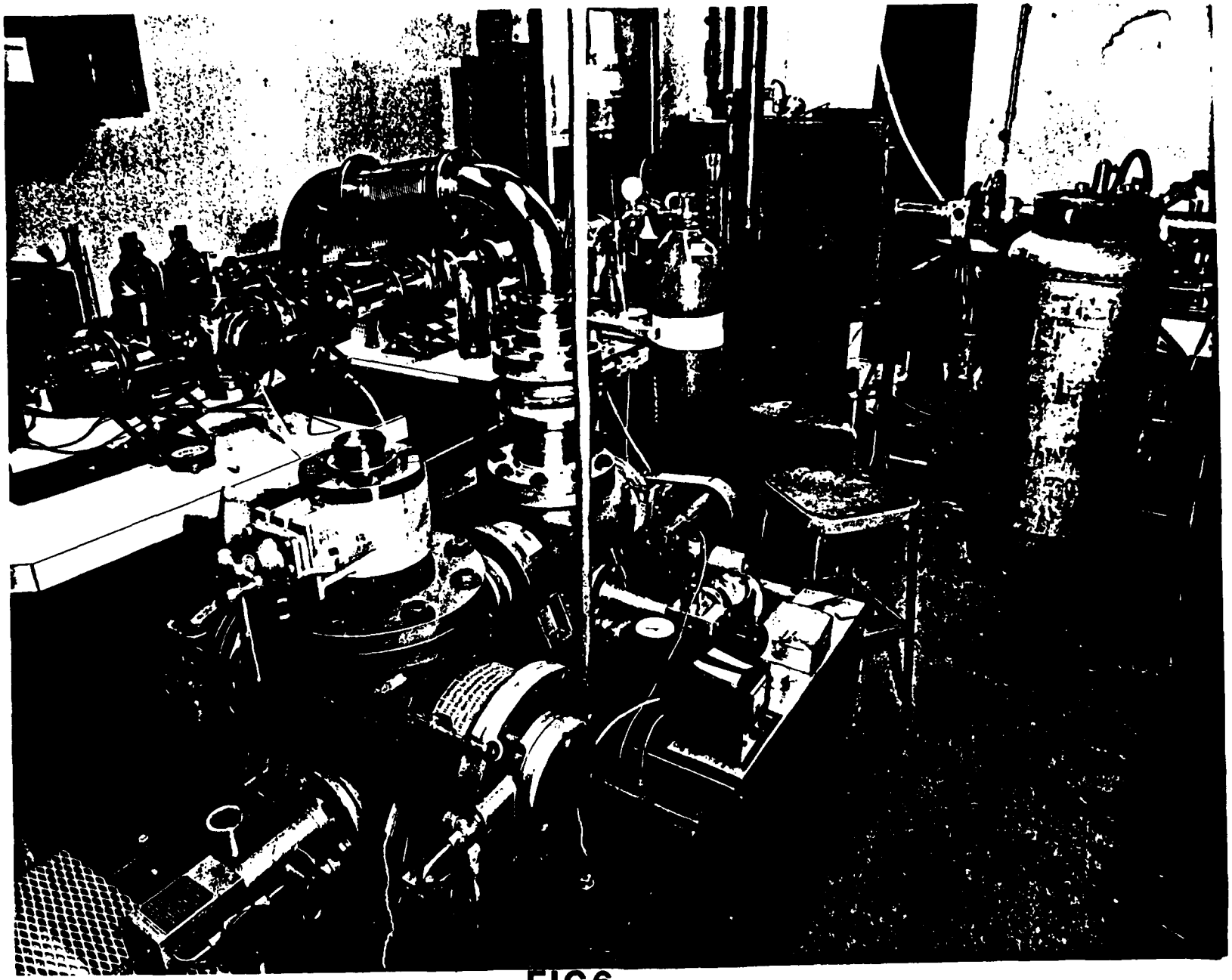

FIG6

IMPLANTER VACUUM SYSTEM

WELL PROCESSED UHV SYSTEM

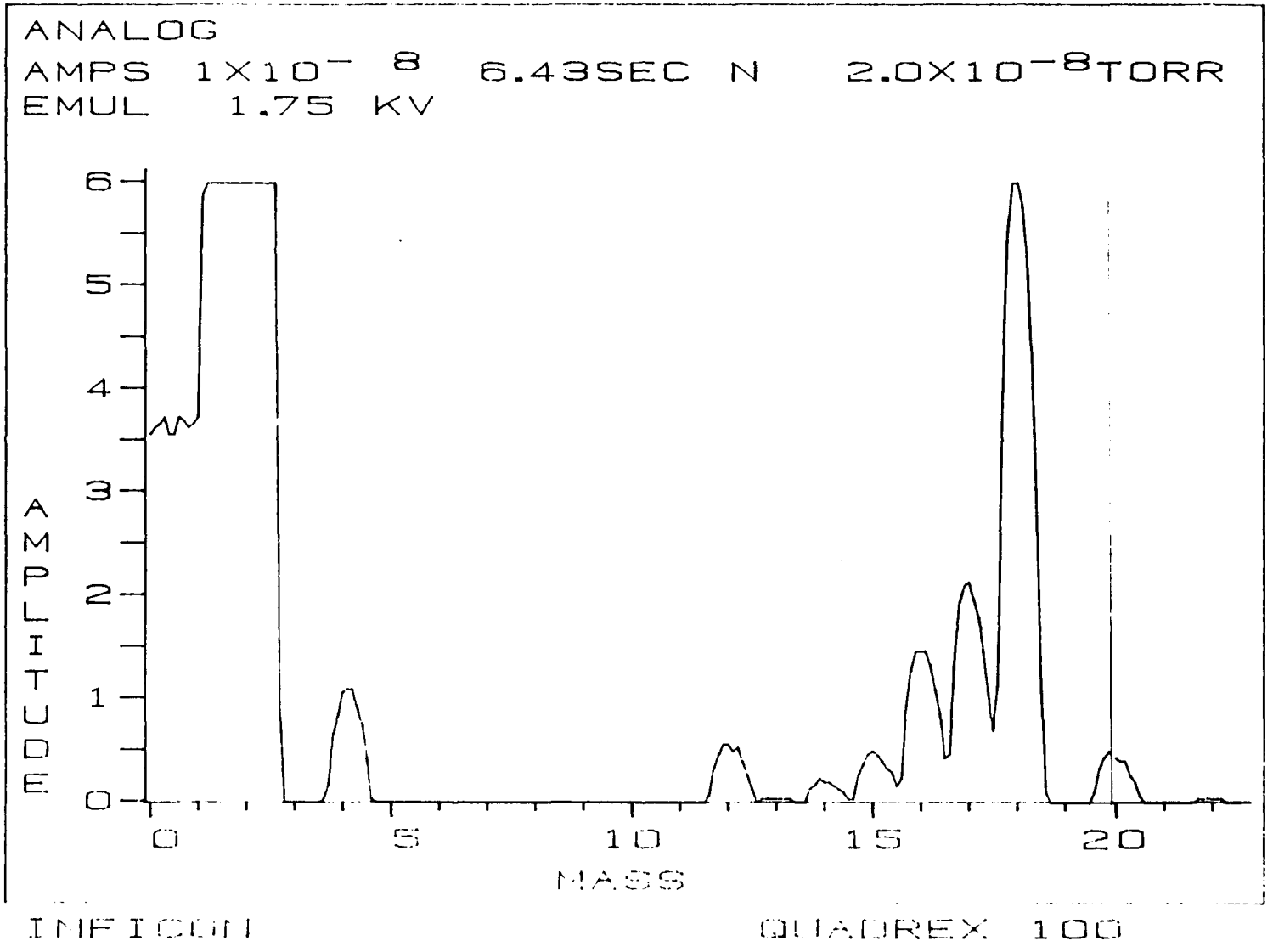

GRAPH1

UHV SYSTEM AT 33x GAIN

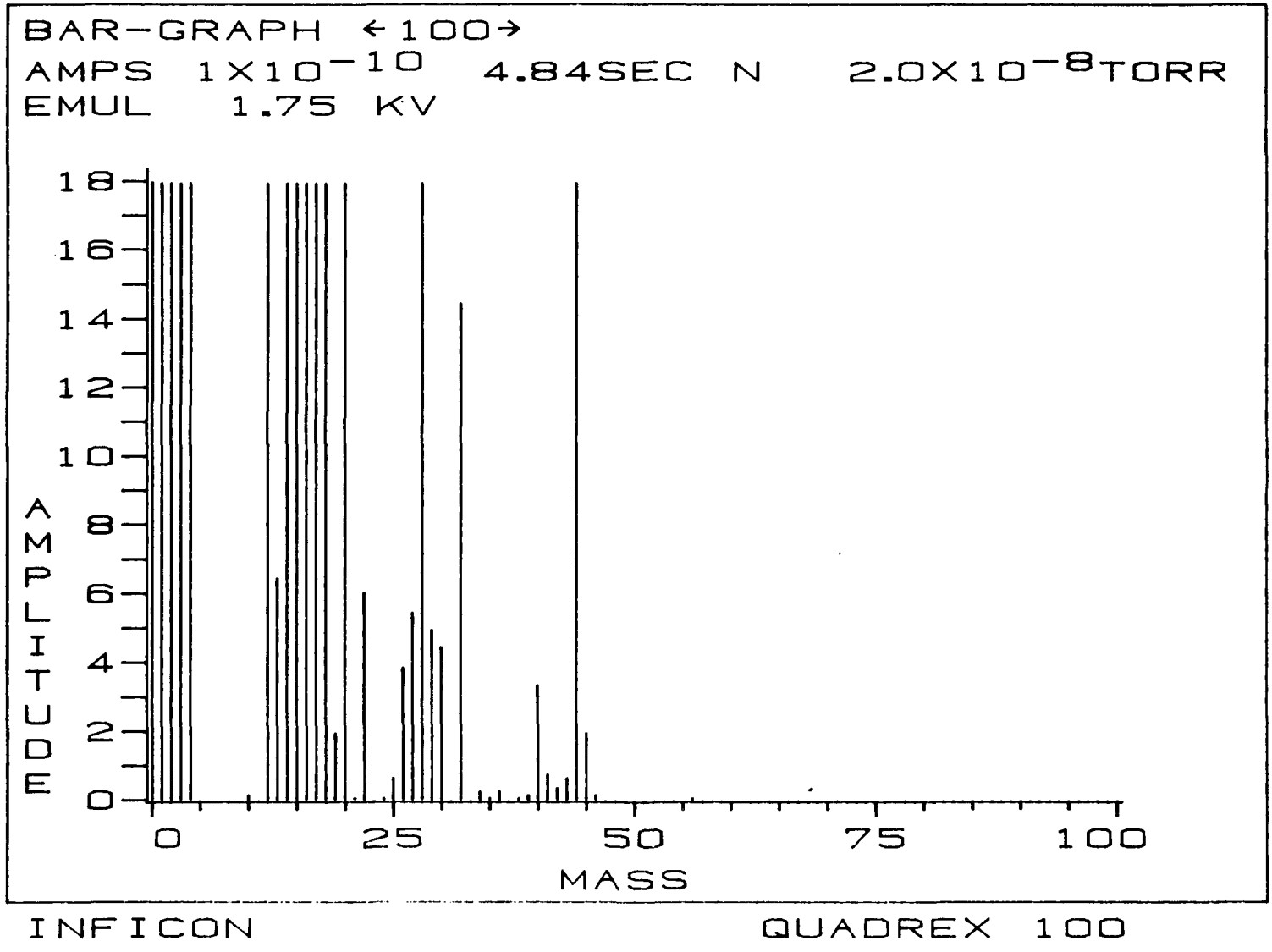

GRAPH2

BAR GRAPH OF UHV SYSTEM

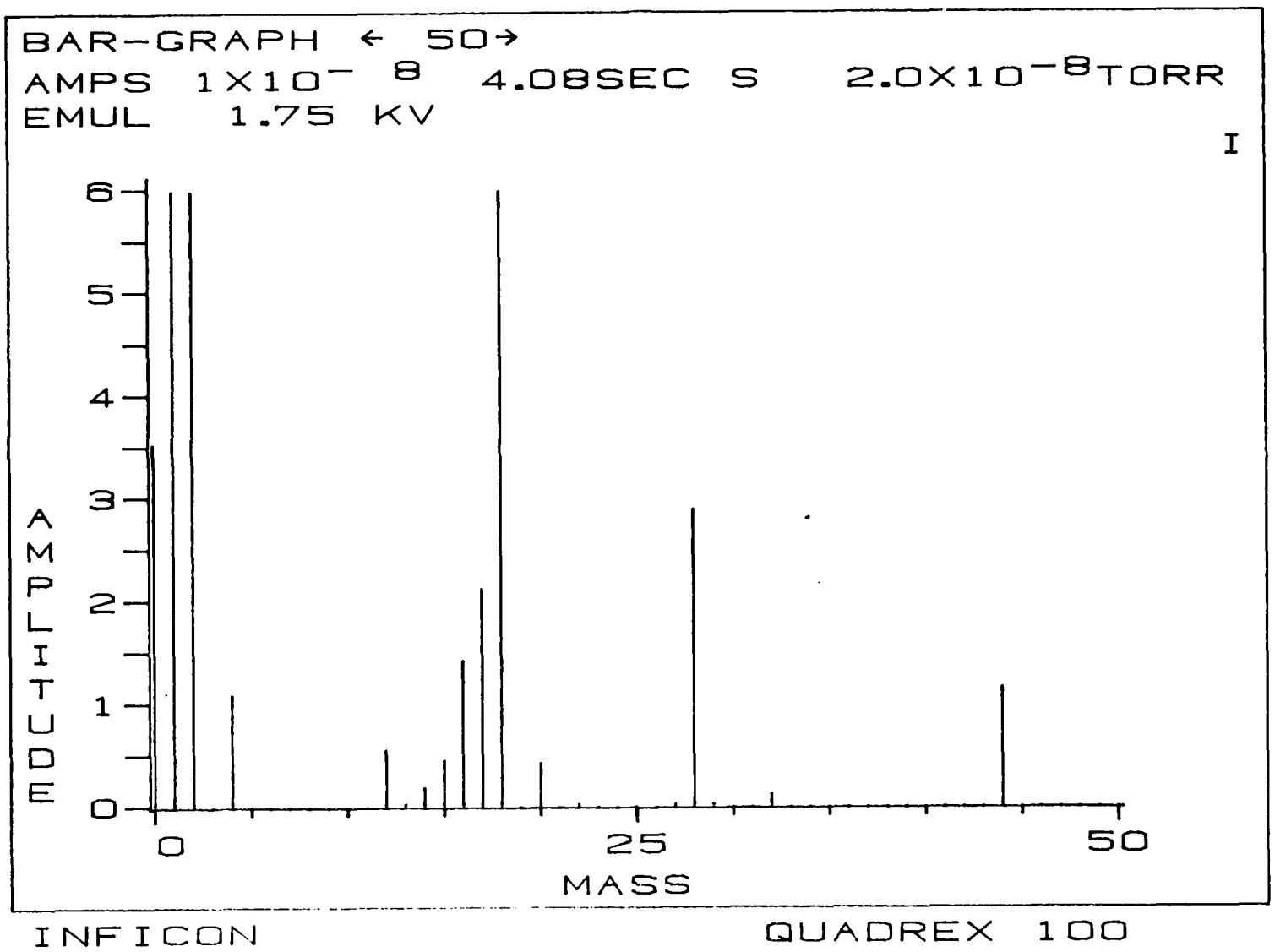

GRAPH3

RAY TRACING PROCEDURE

By Theodore Barrett

INTRODUCTION

A set of source modules and NOS procedures have been prepared to permit easy access to a 3 - dimensional, non-isotropic ray-tracing program (the Jones - Stephenson program). This "system" is designed to be run on a CDC CYBER 170 computer system or equivalent using the NOS operating system. Refer to CDC Manual 60459680, NOS VERSION 2 REFERENCE SET, Volume 3 : System Commands, for details of this operating system.

This report consists of extracts from this system - namely some of the procedures. The "help messages" which constitute part of these procedures help to explain the system and the user interface.

The procedures extracted (either in full or in part) are:

RTPROC
NITPROC
HOLEDOC
DISPROC
TRCPROC
MODPROC
LOKPROC

RTPROC

```
.PROC,RTPROC*M"ray trace menu",OPTION=
(1"initialize",
2"trace",
3"display",
4"modify",
5"look",
6"calculate").
.HELP.
```

The following is general information about the "ray-trace system" (referred to below as RTS). Each procedure used by RTS is of the "interactive form" and much help can be obtained by entering ? when data is requested. In addition the procedure itself can be queried by calling it in the query mode, e.g. NITPROC? such is done by this menu procedure. Additional information on RTS can be obtained from comments within the various source modules. For example PATCH, MEDPLT and RAYPLT contain much info on the coordinate patch concept used by the various displays. The user can look into these modules by selecting 5 which puts the user into an editor (XEDIT). Within editor the command P* will cause the entire module to be displayed while P10 will cause the next 10 lines to be displayed and the line pointer to be moved down 10 lines such that another P10 will cause the next 10 lines to be shown.

It is also possible to make changes to RTS by selecting menu item 4 which again puts the user into XEDIT. After XEDIT is left (by typing the command END) any changes to source modules become permanent. Note that both procedures and source code can be modified this way. Changes to procedures will be effective immediately. If source modules are changed (and NITPROC has previously been invoked) it is probably wise
to issue the commands:

```
LIBRARY,RTLIBS
RETURN,*
```

and then reinitialize using NITPROC.

The following are some general technicalities which the user should observe while using RTS

(1) Procedures may be called in 3 different ways:
query mode (e.g. DISPROC?)
order dependant mode (e.g. DISPROC,NEW)
keyword mode (e.g. DISPROC,TYPE=MEDIUM)
(note that it is not necessary to use the menu procedure RTPROC to call the other procedures)

(2) In the query mode data is given to the procedure in response to a prompt (which contains some lower case letters). The user

```
may respond to the prompt with:
 ?  to obtain info on the data to be entered
 CR ( carriage return ) to accept the default value
 data or $data$ to insert data ( note that data containing
   - or . should be enclosed in $'s
 .  to terminate data entry ( and accept defaults for all
    following parmeters )
 data. or $data$. to insert data and then terminate
 ^T ( T and CTRL simultaneously ) to terminate the procedure.

(3) Data are requested by various non-procedural modules. Such
    requests are always in uppercase and followed by ? on the
    line below the request. If default data are to be used the
    user should respond with CR. ( If the request is for a choice
    of 2 iout of a list of values, the first shown is the default ).
    Numerical values may be one of the follwing forms ( by example )
       3
       3.
       3.0
       3E4 ( 3 x 10**4 )
       3.456E-4
    If several values are requested they should be entered on one
  line and be separated by  one or more blanks or a comma and none
    or more blanks.
.HELP,1
    must be selected before either display or trace
.HELP,2
    to trace rays
.HELP,3
    to display results of tracing and/or the medium
.HELP,4
    to modify a source module in RTLIBS
.HELP,5
    to look at a source module
.HELP,6
  to perform various calculations which may be useful for ray-tracing
.ENDHELP.
ASCII.
IF,OPTION=1,OPT1.
NITPROC?.
ENDIF,OPT1.
IF,OPTION=2,OPT2.
TRCPROC?.
ENDIF,OPT2.
IF,OPTION=3,OPT3.
DISPROC?.
ENDIF,OPT3.
IF,OPTION=4,OPT4.
MODPROC?.
ENDIF,OPT4.
IF,OPTION=5,OPT5.
```

```
LOKPROC?.
ENDIF,OPT5.
IF,OPTION=6,OPT6.
CALPROC.
ENDIF,OPT6.
REVERT,NOLIST.
```

NITPROC

```
.PROC,NITPROC*I"Ray trace initialization",
ID"user name for RTLIBS"=(*N=),
FIELD"mag field module"=(MAGFLD,*N=MAGFLD),
DENSITY"electron density module"=
(CHAPX,SPHEREX,VCHAPX,DCHAPT,*N=CHAPX),
PERT"density perturbation module"=(NONE,WAVE,HOLE,*N=HOLE),
RAYTYPE"ordinary or extraordinary"=(*S2(1$-$),*N=$-1$),
THT"transmitter height"=(*S10(0123456789$.$),*N=0),
TLAT"transmitter latitude"=(*S10(0123456789$.$),*N=$37.83$),
TLON"transmitter longitude"=(*S10(0123456789$.-$),*N=$-76$),
FREQ"frequency (Mhz)"=(*S10(0123456789$.$),*N=8),
AZ"initial azimuth"=(*S10(01231106789$.-$),*N=110),
EL"initial elevation"=(*S10(0123606789$.-$),*N=45),
HOPS"number of hops"=(*S2(0123456789),*N=1),
MGPL"maximum group path length"=(*S5(0123456789),*N=1000),
E0"electron density parm (100)"=(*S10(0123456789$.-$),*N=0),
E1"electron density parm (101)"=(*S10(0123456789$.-$),*N=$6.5$),
E2"electron density parm (102)"=(*S10(0123456789$.-$),*N=300),
E3"electron density parm (103)"=(*S10(0123456789$.-$),*N=62),
E4"electron density parm (104)"=(*S10(0123456789$.-$),*N=$.5$),
E5"electron density parm (105)"=(*S10(0123456789$.-$),*N=0),
E6"electron density parm (106)"=(*S10(0123456789$.-$),*N=0),
E7"electron density parm (107)"=(*S10(0123456789$.-$),*N=0),
E8"electron density parm (108)"=(*S10(0123456789$.-$),*N=0),
P0"perturbation parm (150)"=(*S10(0123456789$.-$),*N=1),
P1"perturbation parm (151)"=(*S10(012326789$.-$),*N=250),
P2"perturbation parm (152)"=(*S10(0123456789$.-$),*N=100),
P3"perturbation parm (153)"=(*S10(0123456789$.-$),*N=$.1$),
P4"perturbation parm (154)"=(*S10(0123456789$.-$),*N=0),
P5"perturbation parm (155)"=(*S10(0123456789$.-$),*N=100),
P6"perturbation parm (156)"=(*S10(0123456789$.-$),*N=100),
P7"perturbation parm (157)"=(*S10(0123456789$.-$),*N=0),
P8"perturbation parm (158)"=(*S10(0123456789$.-$),*N=0),
D0"magnetic field parm (200)"=(*S10(0123456789$.-$),*N=0),
MAP"load map "=(ON,OFF,*N=OFF).
.* REVISION -- JANUARY 9, 1985
.* AUTHOR   -- BARRETT,TB
.* TITLE    -- RAY TRACE INITIALIZATION PROCEDURE
.* DESCRIPTION -- SEE HELP
.HELP.
```

This procedure may be used to create the executable modules for use in ray-tracing and display of the results of ray-tracing. In addition modules which may be used to display the "medium" are created here. If the execution modules have already been created, NITPROC may be called to vary selected parameters for a trace "session" - namely those parameters
which "change slowly" (e.g. transmitter position).

Various assumptions are made as follows:
(1) the ray-trace source modules (including media models) are in a User library called RTLIBS as procedures.
(2) the "specialized" display source modules are in library RTLIBS
(3) the "basis" display source modules are in an update library called NCARPL (the "basis" modules are part of the NCAR graphics package)

The various execution modules are created and put in a library file called TRACLIB. If this library already exists as a permanent file it may
be "attached" before running NITPROC and the procedure is then used to adjust the W-array parameters.

The main mechanism for tailoring the raytrace program for various applications (other than choosing the medium) is via the "W-array". Values are put into this array via "default" (e.g. DATA statements) and via an input file which is read by NITIAL, the main program of the ray trace set of modules. This array (in its form as an input file) is included as part of NITPROC. Some of the W-array values are also parameters of NITPROC.

.HELP,ID.

The ID is the user name of the user library of source files for ray-tracing and display.

.HELP,DENSITY.

The electron density models available and parameters required are:

CHAPX - Chapman layer with tilts, ripples and gradients

```
f/N^2 = f/c^2 * exp(E4*(1-z-e^-z))
  z = (h - h/max) / E3
  f/c^2 = E1^2 * ( 1 + E5*sin( 2*pi*(theta-pi/2)/E6) + E7*(theta-pi/2)
  h/max = E2 + E8*(theta-pi/2)*EARTHR
```

E1 - critical frequency at equator
E2 - height of max. electron density at equator
E3 - scale height (km)
E4 - alpha=.5, beta=1.
E5 - amplitude of periodic variation of f/c with latitude
E6 - period of f/c variation with latitude (rad)
E7 - coefficient of linear variation of f/c with lat (rad**-1)
E8 - tilt of layer (rad)

VCHAPX - Chapman layer with variable scale height

```
f/N^2 = E1^2 * sqrt(tau) * exp( .5*(1 - tau) )
  tau = ( E2/h )^E3
```

```
     E1 = critical frequency ( Mhz )
     E2 = height of max. electron density (km)
     E3 = non-dimensional exponent

 DCHAPT - double tilted alpha-Chapman layer

  f/N^2 = E1^2 * exp( .5*(1-z1 - exp(-z1) ) +
          E4^2 * exp( .5*(1-z2 - exp(-z2) )
    z1 = ( h - hm1)/E3,     z2 = ( h - hm2)/E6
    fc^2 = E1^2*E7*(theta - pi/2)
    fc2^2 = E4^2*E7*(theta - pi/2)
    hm1 = E2 + EARTHR*E8*(dtr)*(theta-pi/2)
    hm2 = E5 +          ""
     rad = pi/180

     E1 = Mhz
     E2 = km
     E3 = km
     E4 = Mhz
     E5 = km
     E6 = km
     E7 = rad^-1
     E8 = deg

HELP,PERT.

     The default electron density perturbation model is NONE.
Other models are:

     WAVE - a gravity wave traveling from north to south pole.

     N = N0*( 1 + del )

     del = P3*exp(-[(r - EARTHR -P1)/P2]^2) *
           cos( 2*pi[P7+(pi/2 - theta)*EARTHR/P5 + (r - EARTHR)/P6])

     P1 - height of max. wave amplitude (km)
     P2 - wave amplitude "scale height" (km)
     P3 - wave perturbation amplitude ( 0 - 1 )
     P4 - horizontal trace velocity
     P5 - horizontal wave length (km)
     P6 - vertical wavelength (km)
     P7 - time in wave periods ( 0 - 1 )

   HOLE - ionospheric hole
          This is a procedure which is run in the inquire mode
     which asks the user for model parameters.
.ENDHELP.
IF,FILE(TRACLIB,.NOT.AS),HAVEIT. Jump to HAVEIT if file exists.
.* create ray trace binaries
IFE,$ID$=$$,USER1.
```

```
ATTACH(RTLIBS)
ELSE,USER1.
ATTACH(RTLIBS/UN=ID)
ENDIF,USER1.
LIBRARY(RTLIBS)
RETURN(RAYTRC)
RAYTRC,COMPILE.     main ray-tracing modules
RETURN,RAYTRC.
RETURN(DENSITY)
IF,$DENSITY$=$CHAPX$,DY.
DENSITY?.
ELSE,DY.
DENSITY,COMPILE.    electron density module
ENDIF,DY.
RETURN,DENSITY.
RETURN(PERT)
IF,$PERT$=$HOLE$,PT.
HOLE?.
ELSE,PT.
PERT,COMPILE.      density perturbation module
ENDIF,PT.
RETURN,PERT.
RETURN,FIELD.
FIELD,COMPILE.      magnetic field module
RETURN,FIELD.
RETURN(RWAF)
RWAF,COMPILE.         read WARRAYF
RETURN,RWAF.
RETURN,GTOD.
GTOD,COMPILE.    various coord. transformation, etc. files follow
RETURN,GTOD.
RETURN,SPHTRI.
SPHTRI,COMPILE.
RETURN,SPHTRI.
RETURN,GETRM.
GETRM,COMPILE.
RETURN,GETRM.
RETURN,VSUBS.
VSUBS,COMPILE.
RETURN,VSUBS.
RETURN,POLTCAR.
POLTCAR,COMPILE.
RETURN,POLTCAR.
RETURN,DISPLA.
DISPLA,COMPILE.
RETURN,DISPLA.
MAKLBLS,COMPILE.
RETURN,MAKLBLS.
VALNUM,COMPILE.
RETURN,VALNUM.
LIBGEN,F=LGO,P=TRACLIB.
```

```
ENDIF,HAVEIT.
.* trace 1 ray to get new W-array
IF,$MAP$=$ON$,MAPP.
RETURN(MAPF)
LDSET(#MAP=E/MAPF,PRESET=0,LIB=TRACLIB)
LIBLOAD(TRACLIB,NITIAL)
EXECUTE(NITIAL)
ELSE,MAPP.
LDSET(PRESET=0,LIB=TRACLIB)
LIBLOAD(TRACLIB,NITIAL)
EXECUTE(NITIAL)
ENDIF,MAPP.
RETURN(TAPE3,TAPE7,LGO)
.DATA,WARRAYF
 NITPROC
1 RAYTYPE /       1 = ordinary, -1 = extraordinary
2 6370. /       surface height ( kilometers )
3 THT   /       transmitter height ( km ) above surface
4 TLAT 1 /      transmitter geographic latitude ( degrees )
5 TLON 1 /      transmitter geographic longitude ( degrees east )
6 FREQ  /       current transmitter frequency
7 FREQ  /       initial transmitter frequency ( MHz )
8 FREQ  /       final transmitter frequency ( MHz )
9 0     /       delta frequency ( Mhz )
10 AZ  1/
11 AZ  1 /   initial ray azimuth ( degrees clockwise from geographic N )
12 AZ  1 /      final ray azimuth
13 0   1 /      delta azimuth
14 EL  1 /      current ray elevation
15 EL  1 /     initial ray elevation ( degrees from tangent to surface )
16 EL  1 /      final ray elevation
17 0   1 /      delta elevation
20 THT  /       receiver height above surface ( kilometer )
21 1    /   non-zero to skip to next frequency on ionosphere penetration
22 HOPS /       max. number of hops
23 1000 /       max. number of steps per hop
24 78.5  1 /    geographic latitude of the north pole ( degrees )
25 291. 1  /geographic longitude of the north pole ( degrees, - = west )
26 20.  /       bottom of ionosphere ( kilometers )
41 3    /       integration type code
42 1.E-4 /      max. allowable single step error
43 50.  /       max. single step error / min. single step error
44 1.   /       initial integration step size ( km )
45 100. /       max. step length (km )
46 1.E-8 /      min. step length (km )
47 .5   /       factor to decrease step length
57 0    /       phase path ( 1 - integrate, 2 - integrate and print )
58 0    /       absorption ( 1 - integrate, 2 - integrate and print )
59 0    /       doppler    ( 1 - integrate, 2 - integrate and print )
60 2    /       path length( 1 - integrate, 2 - integrate and print )
71 0    /       integrations steps between printout ( 0 -> use W(23) )
```

```
72 3     /        output control ( bits  B0-TAPE7,B1-TAPE3,B2-OUTPUT )
73 0     /        additional control for intermediate points
80 0     /        delta azimuth for bundle traces
81 0     /        delta elevation for bundle traces
82 TLAT 1 /       receiver geographic latitude ( used for displays )
83 TLON 1 /       receiver geographic longitude
90 MGPL /      max. group path length ( if non-zero do not trace beyond )
98 0     /        if non-zero, reduce number of el. angles on next azimuth
.*                  if the ray penetrated on this azimuth.
99 3     /        input check control
100 E0   /        ELECTX parameter ( must see particular model for use )
101 E1   /        ELECTX parameter ( must see particular model for use )
102 E2   /        ELECTX parameter ( must see particular model for use )
103 E3   /        ELECTX parameter ( must see particular model for use )
104 E4   /        ELECTX parameter ( must see particular model for use )
105 E5   /        ELECTX parameter ( must see particular model for use )
106 E6   /        ELECTX parameter ( must see particular model for use )
107 E7   /        ELECTX parameter ( must see particular model for use )
108 E8   /        ELECTX parameter ( must see particular model for use )
150 P0 /        ELECT1 parameter
151 P1 /
152 P2 /
153 P3 /
154 P4 /
155 P5 /
156 P6 /
157 P7 /
158 P8 /
200 D0   /        MAGF paramete
201 .80 /         gyrofrequency at equator ( MHz ) - used by DIPOLY
249 1984 /        time in years for which accurate field is required
.*                  if zero it is set to 1965 - used with IGRFMAG.
```

HOLEDOC

```
.PROC,HOLEDOC*I" Ionospheric hole documentation",
COMPILE" compile hole "=(NO,YES,*N=NO).
.* REVISION -- DECEMBER 5, 1984
.* AUTHOR   -- BARRETT,TB
.* TITLE    -- HOLE DOCUMENTATION
.HELP.
```

Rays may be traced in an ionosphere which contains a "hole" in an otherwise "normal" ionosphere are described. The purpose of this exercise in ray tracing is to attempt to explain the ionograms observed at the Wallops Island ionosonde shortly after the release of 20 kg of SF6 at an altitude of 348 km. The Wallops Island observatory is located at 37 deg 49.8 min N, 76 deg 00 min W and the release coordinates are 37 deg 06 min N, 74 deg 00 min W. The released SF6 ionizes by electron attachment and rapidly "stabilizes" with the subsequent formation of ionized SF5 + F . Almost all of the electrons in the vicinity of the release become bound with the result that "hole" appears in the ionosphere. According to calculations by Berhardt [Chemistry and Dynamics of SF6 Injections into the F-Region, P. A. Berhardt, Project IMS, Compiled Participant Submissions and General Information, AFGL, Hanscom Air Force Base] the depletion region is approximately 100 km in diameter 1 minute after release and up to 200 km in diameter 10 minutes after release. The neutral SF6 concentration is such that under gravity SF6 diffuses downwards and continues to remove electrons from the ionosphere. Thus what is orignally a spherical depletion region becomes a cylindrical one (assuming that electrons do not diffuse back into the depletion region from the undisturbed ionosphere). The initial electron density model used for ray-tracing is a spherical perturbation of an ambient double or single Chapman layer (which only varies with height).

2. The electron density model

The normalized electron density, X, is perturbed by a multiplicative function f(l,a,b) where l is the distance from the center of the perturbed ionosphere and a and b are parameters which can be input by the user to

```
change the height and diameter of the spherical perturbation. The
function
f is made smooth such that it has continuous first derivatives
everywhere.
Thus we have:

        X(r,t,p) = X/a(r,t,p) * f(l) ,
        r = radial coordinate
        t = theta
        p = phi
        X/a = ambient ionosphere
        f << 1 for 0 < l < L
        f = 1 l >= L.
        l = [ r**2 + r/0**2 - 2*r( sin(t)*cos(p)*x/0 + sin(t)*sin(p)*y/0
              + cos(t)*z/0 ]**1/2
        r/0 = radial coordinate of the center of the disturbance
        x/0,y/0,z/0 = Cartesian coordinates of the center of the
disturbance.

    The explicit form chosen for f is

        f(l) = ( sin(al) )**n     0 <= l <= pi/(2*a)
             = 1                  elsewhere.

    Thus
        f' = df/dl = a*n*cos(al)*( sin(al))**(n-1)  0 <= l <= pi/(2a)
           = 0                                      elsewhere.

    In addition to X itself the derivatives of X wrt r,t,p are required.
They are as follows:

        ( let A stand for the ambient X/a)

    dX/dr = dA/dr*f + A * df/dl*dl/dr,
    dX/dt = A * df/dl*dl/dt  ( since the ambient varies only with
height,
    dX/dp = A * df/dl*dl/dp,
    dl/dr = l**(-1) * ( r - sin(t)cos(p)*x/0 - sin(t)sin(p)*y/0 -
cos(t)*z/0)
    dl/dt = -r*l**(-1) * (cos(t)cos(p)*x/0 + cos(t)sin(p)*y/0 -
sin(t)*z/0)
    dl/dp = -1r*l**(-1) * (-sin(t)sin(p)*x/0 + sin(t)cos(p)*y/0)

 For samll a*l df/dl*l**(-1) == a**2 * n * (a*l)**(n-2).
( Assume that n >= 2 )

.ENDHELP.
IF,$COMPILE$=$YES$,CMP.
IF,(FILE(RTLIBS,.NOT.AS),GETRT.
ATTACH(RTLIBS)
ENDIF,GETRT.
```

```
LIBRARY(RTLIBS)
HOLE.
ENDIF,CMP.
```

DISPROC

```
.PROC,DISPROC*I"Display procedure",
NEW" new coordinate patch"=(NEW,OLD,*N=OLD),
TYPE" display type"=(MEDIUM,PROFILE,RAY,*N=RAY),
DEVICE" plot device"=(CRT,PEN,PRNT,*N=CRT).
.*
.* REVISION --JANUARY 14, 1985
.* AUTHOR4  -- BARRETT,TB
.* TITLE    -- RAY TRACE DISPLAY
.* DESCRIPTION -- SEE HELP
.HELP.
```

This procedure may be used to display "the medium" or one or more rays, or both. It assumes that NITPROC has been run to produce the library of "execution" modules required for display and the WARRAY file which contains certain information which may be used for defining coordinates and possibly the medium. If rays are to be displayed, the procedure TRCPROC should have been run. The medium may be displayed as contours, halftones or vectors if MEDIUM is chosen or as a profile through the center of the cordinate patch if PROFILE is chosen.

```
.HELP,NEW.
```

If NEW is specified, a new coordinate patch is created according to data input by the user when PATCH is run. If the "patch" file, PATCHF does not exist, PATCH is run even if NEW is not specified.

```
.HELP,TYPE.
```

If MEDIUM is specified, the ray-trace medium (as "specified" by modules in TRACLIB, created by NITPROC) is plotted using program MEDPLT and the appropriate NCAR plot modules. If RAY is specified, RAYPLT is executed to produce a ray projection plot. If PROFILE is specified medium profiles (through the center of the coordinate patch) are drawn.

```
.HELP,DEVICE.
```

The DEVICE is the device on which the plot is to appear. If you are running this procedure at a Tektronix 4014 type terminal you may use the DEVICE type CRT. Otherwise use PEN. For a quick look at a "plot" at a non-graphics terminal, a device type of PRNT may be used. In this case no plot is done. A pseudo plot appears at the terminal.

```
.ENDHELP.
RETURN,LGO,COMPILE,TAPE8.
ASCII.
```

```
IF,FILE(RTLIBS,.NOT.AS).OR.FILE(TRACLIB,.NOT.AS),GETRT.
NOTE.* PLEASE RUN NITPROC, THE INITIALIZATION PROCEDURE
REVERT,NOLIST.
ENDIF,GETRT.
LIBRARY(TRACLIB,RTLIBS)
IF,FILE(NCARLIB,.NOT.AS),GETNCAR.
GETP,NCARLIB.
ENDIF,GETNCAR.
IF,FILE(PATCHF,.NOT.AS).OR.$NEW$=$#NEW$,NEWP.
IF,FILE(ROUTEF,AS),FINPLT.
.* the user may have forgotten to finish the plot
NOTE.* THE PLOT MAY NOT BE COMPLETE
NOTE.* IF SO, RERUN DISPROC WITH THE OLD PATCH
RETURN,ROUTEF.
REVERT,NOLIST.
ENDIF,FINPLT.
IF,FILE(PATGO,.NOT.AS),MAKAGO.
ATTACH(OLDPL=NCARPL/UN=PLIB)
UPDATE(Q,D,8,I=RAYPLOT,L=0)
RETURN(OLDPL)
GETP,BLOCK.
RETURN,PATCH.
PATCH,COMPILE.
RETURN,PATCH.
FTN(I,OPT=1,L=0)
RETURN(COMPILE)
LDSET(PRESET=0,LIB=NCARLIB/TRACLIB)
LOAD(BLOCK)
LOAD(LGO)
NOGO(PATGO,PATCH)
RETURN,LGO.
ENDIF,MAKAGO.
REWIND(WARRAYF)
PATGO.
ENDIF,NEWP.
IF,$TYPE$=$MEDIUM$,MED.
IF,FILE(MEDGO,.NOT.AS),MAKMGO.
ATTACH(OLDPL=NCARPL/UN=PLIB)
UPDATE(Q,D,8,I=MEDPLOT,L=0)
RETURN(OLDPL)
GETP,BLOCK.
RETURN,MEDPLT.
MEDPLT,COMPILE.
RETURN,MEDPLT,MEDPLOT.
FTN(I,OPT=1,L=0)
RETURN,COMPILE.
LDSET(PRESET=0,LIB=NCARLIB/TRACLIB)
LOAD(BLOCK)
LOAD(LGO)
NOGO(MEDGO,MEDPLT)
ENDIF,MAKMGO.
```

```
MEDGO.
ENDIF,MED.
IF,$TYPE$=$RAY$,RAY.
IF,FILE(RAYGO,.NOT.AS),MAKRGO.
ATTACH(OLDPL=NCARPL/UN=PLIB)
REWIND(RAYPLOT)
UPDATE(Q,D,8,I=RAYPLOT,L=0)
RETURN(OLDPL)
GETP,BLOCK.
RETURN,RAYPLT.
RAYPLT,COMPILE.
RETURN,RAYPLT.
FTN(I,OPT=1,L=0)
RETURN(COMPILE)
LDSET(PRESET=0,LIB=NCARLIB/TRACLIB)
LOAD(BLOCK)
LOAD(LGO)
NOGO(RAYGO,RAYPLT)
ENDIF,MAKRGO.
RAYGO.
ENDIF,RAY.
IF,$TYPE$=$PROFILE$,PRO.
IF,FILE(PROGO,.NOT.AS),MAKPGO.
ATTACH(OLDPL=NCARPL/UN=PLIB)
REWIND(RAYPLOT)
UPDATE(Q,D,8,I=RAYPLOT,L=0)
RETURN(OLDPL)
GETP,BLOCK.
RETURN,PROPLT.
PROPLT,COMPILE.
RETURN,PROPLT.
FTN(I,OPT=1,L=0)
RETURN(COMPILE)
LDSET(PRESET=0,LIB=NCARLIB/TRACLIB)
LOAD(BLOCK)
LOAD(LGO)
NOGO(PROGO,PROPLT)
ENDIF,MAKPGO.
PROGO.
ENDIF,PRO.
IF,FILE(TAPE8,.NOT.AS),NOFILE.
NOTE.*NO POINTS ON COORDINATE PATCH
REVERT.
ENDIF,NOFILE.
IF,$DEVICE$=$PRNT$,PRT.
RETURN(PRB,LGO)
FTN5(I=PREPARE,B=PRB,L=0)
RETURN(PREPARE)
PRB.
RETURN(PRB)
IF,FILE(DISB,.NOT.AS),MAKDIS.
```

```
LDSET(PRESET=0,LIB=TRACLIB)
LIBLOAD(TRACLIB,DISPLA1)
NOGO(DISB,DISPLA1)
ENDIF,MAKDIS.
DISB.
REVERT.
ENDIF,PRT.
REWIND(TAPE8)
GET,NCP=NCPLTRV/UN=PLIB.
IF,$DEVICE$=$CRT$,TEK.
ATTACH(PEN=TEKSIM/UN=PLIB)
BANPROC.
LDSET(PRESET=0,LIB=PEN/NCARLIB)
NCP(BANNER)
ELSE,TEK.
GET,PEN=OFFPEN4/UN=PLIB.
BANPROC,#DEVICE=PEN.
LDSET(PRESET=0,LIB=PEN/NCARLIB)
NCP(BANNER)
IF,FILE(ROUTEF,AS),OVL.
ROUTE(TAPE39,DC=PL,ID=62)
ENDIF,OVL.
ENDIF,TEK.
RETURN(BANNER,NCP)
RETURN,PEN.
EXIT.
REVERT,NOLIST.
```

TRCPROC

```
.PROC,TRCPROC*I"Ray-trace procedure",
MODE" continuous or interrupted"=(C,I,*N=I),
R1" report event 1"=(NULL,XMTR,RCVR,PENETRAT,APOGEE,PERIGEE,$MAX LAT$,
 $MAX LONG$,$MIN DIST$,$WAVE REV$,$GRND REF$,$PAST 90.$,$90 DEG.$,
 $STEP MAX$,$PATH MAX$,$OVERDENS$,$ $,$ENTR ION$,$EXIT ION$,$BACK UP1$,
 $BACK UP2$,$BACK UP3$,$GRAZE 0$,$GRAZE 1$,$PLOT PT$,*N=APOGEE),
R2" report event 1"=(NULL,XMTR,RCVR,PENETRAT,APOGEE,PERIGEE,$MAX LAT$,
 $MAX LONG$,$MIN DIST$,$WAVE REV$,$GRND REF$,$PAST 90.$,$90 DEG.$,
 $STEP MAX$,$PATH MAX$,$OVERDENS$,$ $,$ENTR ION$,$EXIT ION$,$BACK UP1$,
 $BACK UP2$,$BACK UP3$,$GRAZE 0$,$GRAZE 1$,$PLOT PT$,*N=RCVR),
R3" report event 1"=(NULL,XMTR,RCVR,PENETRAT,APOGEE,PERIGEE,$MAX LAT$,
 $MAX LONG$,$MIN DIST$,$WAVE REV$,$GRND REF$,$PAST 90.$,$90 DEG.$,
 $STEP MAX$,$PATH MAX$,$OVERDENS$,$ $,$ENTR ION$,$EXIT ION$,$BACK UP1$,
 $BACK UP2$,$BACK UP3$,$GRAZE 0$,$GRAZE 1$,$PLOT PT$,*N=NULL),
R4" report event 1"=(NULL,XMTR,RCVR,PENETRAT,APOGEE,PERIGEE,$MAX LAT$,
 $MAX LONG$,$MIN DIST$,$WAVE REV$,$GRND REF$,$PAST 90.$,$90 DEG.$,
 $STEP MAX$,$PATH MAX$,$OVERDENS$,$ $,$ENTR ION$,$EXIT ION$,$BACK UP1$,
 $BACK UP2$,$BACK UP3$,$GRAZE 0$,$GRAZE 1$,$PLOT PT$,*N=NULL),
F" starting frequency"=(*S5(0123456789$.$),*N=NULL),
FE" ending frequency"=(*S5(0123456789$.$),*N=NULL),
DF" frequency increment"=(*S5(0123456789$.$),*N=0),
E" starting elevation"=(*S10(0123456789$.$),*N=NULL),
EE" ending elevation"=(*S10(0123456789$.$),*N=NULL),
DE" elevation increment"=(*S10(0123456789$.$),*N=0),
A" starting azimuth"=(*S10(0123456789$.$),*N=NULL),
AE" ending azimuth"=(*S10(0123456789$.$),*N=NULL),
DA" azimuth increment"=(*S10(0123456789$.$),*N=0).
.*
.* REVISION -- JANUARY 10, 1985
.* AUTHOR   -- BARRETT,TB
.* TITLE    -- RAY TRACE PROCEDURE
.* DESCRIPTION -- See HELP
.*
.HELP.
```

This procedure assumes that NITPROC has been run to produce the "primary" W-array file and TRACLIB, the library of ray-trace modules. It provides a means of entering the most commonly changed ray-trace parameters (frequency, initial ray direction) and also provides some control over the amount of ray summary data output.

```
.HELP,MODE.
```

There are 2 modes of operation possible, CONTINUOUS (C) and INTERRUPTED
(I). In CONTINUOUS mode all rays are traced without interruption. In INTERRUPTED mode the procedure stops after each ray is traced. This

```
allows
the user the opportunity of displaying the ray before continuing. Then
TRCPROC may be invoked again ( with no parameters ) to trace the next
ray in the sequence.

.HELP,R1.

    The parameters R1, R2, R3, R4 may be given values as shown in the
acceptable list. If NULL is chosen, no ray report is output. However,
procedure RPTPROC may be invoked at any time to give a report on all
rays traced during any given session.

.HELP,F .

    The parameters F, FE, DF etc. if given values replace values in
the transient W-array file. If they are not given values, existing
values are used.

.ENDHELP.
IF,FILE(TRACLIB,.NOT.AS).OR.FILE(WARRAYF,.NOT.AS),NOGO.
NOTE.* PLEASE INVOKE NITPROC TO CREATE TRACLIB
REVERT.
ELSE,NOGO.
LIBRARY(TRACLIB,RTLIBS)
ENDIF,NOGO.
.* compile SUMRIZ
RETURN(SUMB)
FTN5(I=SUMRIZ,B=SUMB,L=0)
RETURN(SUMRIZ)
.* if interrrupt mode then use transaction record processor to update
.* WARRAYF
IF,$MODE$=$C$,MODEC.
RETURN(TRANSF)
ENDIF,MODEC.
.* if the transaction record does not exist, create it
IF,FILE(TRANSF,.NOT.AS),CRTR.
RETURN(CRTB)
FTN5(I=CRTRANS,B=CRTB,L=0)
CRTB.
RETURN(CRTRANS,CRTB)
ELSE,CRTR.
IF,FILE(TRB,.NOT.AS).AND.$MODE$=$I$,MKTRB.
FTN5(I=TRANACT,B=TRB,L=0)
RETURN(TRANACT)
ENDIF,MKTRB.
TRB.
.* Already have a transaction record. If at BOI then no more to do.
IF,FILE(TRANSF,BOI),ATEND.
RETURN(TRANSF,CRTB)
NOTE.* ALL RAYS TRACED. RERUN TRCPROC WITH NEW PARAMETERS.
REVERT.
```

```
ENDIF,ATEND.
ENDIF,CRTR.
RETURN,TAPE7,TAPE3.
LDSET(PRESET=0)
LIBLOAD(TRACLIB,NITIAL)
EXECUTE(NITIAL)
.* report
SUMB.
.* exit if get error in tracing
EXIT.
IF,FILE(TAPE7,AS),TP7.
SUMB.
ENDIF,TP7.
REVERT.
```

```
.DATA,CRTRANS
        PROGRAM CRTRANS( WARRAYF, TRANSF, OUTPUT )
        BOOLEAN WARRAYF, TRANSF
        LOGICAL RWAF
        PARAMETER ( DTR = 1.745329252E-2 )
        COMMON/WW/ ID(10), W0, W(400)
        EQUIVALENCE
     $       ( FR, W(7) ),
     $       ( FRE, W(8) ),
     $       ( DFR, W(9) ),
     $       ( AZ, W(11) ),
     $       ( AZE, W(12) ),
     $       ( DAZ, W(13) ),
     $       ( EL, W(15) ),
     $       ( ELE, W(16) ),
     $       ( DEL, W(17) )
        DATA WARRAYF/L"WARRAYF"/, TRANSF/L"TRANSF"/
C CREATES THE TRANSACTION RECORD
C READ IN THE W-ARRAY
        IF (.NOT. RWAF(1000, DUM )) STOP
        IF ( "F" .EQ. "NULL" ) THEN
            PF = FR
            PFE = FRE
            PDF = DFR
            FC = FR
            ELSE
            PF = F
            IF ( "FE" .EQ. "NULL" ) THEN
                PFE = F
                ELSE
                PFE = FE
                ENDIF
            PDF = DF
            FC = F
            ENDIF
        IF ( "E" .EQ. "NULL" ) THEN
            PE = EL
            PEE = ELE
            PDE = DEL
            EC = EL
            ELSE
            PE = E*DTR
            IF ( "EE" .EQ. "NULL" ) THEN
                PEE = E*DTR
                ELSE
                PEE = EE*DTR
                ENDIF
            PDE = DE*DTR
            EC = PE
            ENDIF
        IF ( "A" .EQ. "NULL" ) THEN
```

```
            PA = AZ
            PAE = AZE
            PDA = DAZ
            AC = AZ
            ELSE
            PA = A*DTR
            IF ( "AE" .EQ. "NULL" ) THEN
                PAE = A*DTR
                ELSE
                PAE = AE*DTR
                ENDIF
            PDA = DA*DTR
            AC = PA
            ENDIF
        IF ( "MODE" .EQ. "I" ) THEN
            WRITE( TRANSF ) PF, PFE, PDF, FC, PE, PEE, PDE, EC,
     $                  PA, PAE, PDA, AC
            FR = FC
            FRE = FC
            DFR = 0.
            AZ = AC
            AZE = AC
            DAZ = 0.
            EL = EC
            ELE = EC
            DEL = 0.
            ELSE
            FR = FC
            FRE = PFE
            DFR = PDF
            AZ = AC
            AZE = PAE
            DAZ = PDA
            EL = EC
            ELE = PEE
            DEL = PDE
            ENDIF
        REWIND WARRAYF
            WRITE( WARRAYF, '(8A10)' ) ( ID(I), I = 1, 8 )
            DO 120 I = 1, 400
                WRITE( WARRAYF, * ) I, W(I), '/'
120             CONTINUE
        END
```

```
.DATA,TRANACT
        PROGRAM TRANACT( TRANSF, WARRAYF, OUTPUT )
C UPDATES THE TRANSACTION RECORD
        BOOLEAN TRANSF, WARRAYF
        LOGICAL RWAF
        COMMON/WW/ ID(10), W0, W(400)
        EQUIVALENCE
     $       ( FR, W(7) ),
     $       ( FRE, W(8) ),
     $       ( DFR, W(9) ),
     $       ( AZ, W(11) ),
     $       ( AZE, W(12) ),
     $       ( DAZ, W(13) ),
     $       ( EL, W(15) ),
     $       ( ELE, W(16) ),
     $       ( DEL, W(17) )
        DATA TRANSF/L"TRANSF"/, WARRAYF/L"WARRAYF"/
        IF ( .NOT. RWAF( 1000, DUM ) ) STOP
        REWIND TRANSF
        READ( TRANSF, END=100 ) PF, PFE, PDF, FC, PE, PEE, PDE, EC,
     $                  PA, PAE, PDA, AC
        EC = EC + PDE
        IF ( EC .GT. PEE ) THEN
            EC = PE
            AC = AC + PDA
            IF ( AC .GT. PAE ) THEN
                  AC = PA
                FC = FC + PDF
                IF ( FC .GT. PFE ) THEN
                    FC = PF
                    ENDIF
                ENDIF
            ENDIF
        REWIND TRANSF
        IF ((FC .EQ. PF).AND.(AC .EQ. PA).AND.(EC .EQ. PE)) THEN
            STOP
            ELSE
            WRITE( TRANSF ) PF, PFE, PDF, FC, PE, PEE, PDE, EC,
     $                     PA, PAE, PDA, AC
            FR = FC
            FRE = FC
            DFR = 0.
            AZ = AC
            AZE = AC
            DAZ = 0.
            EL = EC
            ELE = EC
            DEL = 0.
            REWIND WARRAYF
            WRITE( WARRAYF, '(8A10)' ) ( ID(I), I = 1, 8 )
            DO 120 I = 1, 400
```

```
                WRITE( WARRAYF, * ) I, W(I), '/'
120             CONTINUE
            ENDIF
      STOP
100   PRINT *, ' NO TRANSACTION RECORD '
       END
```

```
DATA,SUMRIZ
      PROGRAM SUMRIZ( TAPE7, REPORTF, OUTPUT )
C EXTRACTS RAY DATA FROM TAPE7 AND PRINTS IT. ALSO ADDS
C TAPE7 DATA TO THE RAY REPORT FILE, REPORTF.
C UP TO 4 "REASONS" MAY BE USED FOR EXTRACTING A RAY
      PARAMETER ( RTD = 5.729577951E1 )
      REAL W(400), S(12)
      REAL RES(4)
C THE REASONS TO MATCH
      INTEGER ID(10)
      BOOLEAN REPORTF
      EQUIVALENCE ( EARTHR, W(2) )
      DATA REPORTF/L"REPORTF"/
      DATA N/0/, NPR/0/

C REASONS ARE FILLED IN BY THE PROCEDURE
      DATA RES/"R1", "R2", "R3", "R4"/


      REWIND 7
 100  READ( REPORTF, END = 110 )
      GOTO 100
 110  READ( 7, END = 120 ) ID, W, NTYPE, N
      IF ( RES(1) .NE. "NULL" ) WRITE( *, 5 )
      WRITE( REPORTF ) ID, W, NTYPE, N
 140  READ( 7, END=120 ) R, THETA, PHI, NHOP, WHY, GPL,
     $  ( S(I), I=4,N ), PSI, FR, AZ, EL
      IF ( WHY .EQ. "XMTR" ) THEN
           TH0 = THETA
           PH0 = PHI
           ENDIF
      WRITE( REPORTF ) R, THETA, PHI, NHOP, WHY, GPL,
     $     ( S(I), I = 1,N ), PSI, FR, AZ, EL
      IF ( NHOP .EQ. -1 ) THEN
           IF ( NPR .EQ. 0 .AND. RES(1) .NE. "NULL" ) THEN
                    CALL SPHTRI( PHIO-PH0, THETAO, TH0, D1, RNG, D2 )
                    H = RO - EARTHR
                    WRITE( *, 10 ) WHYO, FO, ELO*RTD, AZO*RTD, H,
     $                   RNG*EARTHR, GPL
                    ENDIF
             IF ( NHOP .EQ. -2 ) STOP
             NPR = 0
             GOTO 140
           ENDIF
C SAVE VALUES IN CASE GET TRAILER RECORD
      RO = R
      THETAO = THETA
      PHIO = PHI
      WHYO = WHY
```

```
      GPLO = GPL
      FO = FR
      AZO = AZ
      ELO = EL
      CALL SPHTRI( PHI-PH0, THETA, TH0, D1, RNG, D2 )
      DO 150 I = 1, 4
          IF ( RES(I) .EQ. WHY ) THEN
              NPR = NPR + 1
              WRITE( *, 10 ) WHY, FR, EL*RTD, AZ*RTD,
     $         R - EARTHR, RNG*EARTHR, GPL
              ENDIF
150       CONTINUE
        GOTO 140
120   IF ( N .EQ. 0 ) THEN
          PRINT *, ' EMPTY TAPE7'
          ELSE
          PRINT *, ' PREMATURE EOF ON TAPE7'
          ENDIF
5     FORMAT( 8X,'  FR',T18,'EL',T26,'AZ',T35,'HT',T44,'RNG',T56,'GPL')
10    FORMAT( A8, 1X, F7.4, 1X, F7.4, 1X, F9.5, 1X, F6.2, 1X, G12.4,
     $         1X, G12.4)
      END
EOI.  0 FILES. 1 RECS. 1347 WORDS.
```

MODPROC

```
.PROC,MODPROC*I" Modify a ray trace source module ",
NAME" module name"=(*S7(ABCDEFGHIJKLMNOPQRSTUVWXYZ0123456789),*N=),
OWN" input OWN if you own RTLIBS"=(OWN,*N=).
.HELP.
   A module in RTLIBS may be modified and replaced in RTLIBS
with the help of this procedure. For a list of module names
reply to the prompt with CR and then rerun this procedure.
.HELP,NAME.
   The name of the module to be modified must be a procedure
in RTLIBS.
.ENDHELP.
IF,$NAME$=$$,HLP.
CATALOG,RTLIBS,U,R.
ELSE,HLP.
LIBRARY.
IF,FILE(RTLIBS,.NOT.WR).AND.$OWN$=$$,OK.
NOTE.* making copy of file RTLIBS for local use.
REWIND(RTLIBS)
RETURN(RTTEMP)
DEFINE,RTTEMP.
COPY,RTLIBS,RTTEMP.
RETURN(RTLIBS)
CHANGE(RTLIBS=RTTEMP)
ENDIF,OK.
RETURN(RTLIBS)
ATTACH(RTLIBS/M=W)
RETURN,TXT.
GTR,RTLIBS,TXT.PROC/NAME
NOTE.* type HELP if need help in XEDIT, END to exit
XEDIT,TXT,AS.
LIBEDIT,P=RTLIBS,B=TXT,I=0,C,U.
RETURN,TXT.
LIBRARY(RTLIBS)
ENDIF,HLP.
```

LOKPROC

```
.PROC,LOKPROC*I" Display a ray trace source module ",
NAME" module name"=(*S7(ABCDEFGHIJKLMNOPQRSTUVWXYZ0123456789),*N=).
.HELP.
 A module in RTLIBS may be displayed using XEDIT
with the help of this procedure. For a list of module names
reply to the prompt with CR and then rerun this procedure.
.HELP,NAME.
   The name of the module to be modified must be a procedure
in RTLIBS.
.ENDHELP.
IF,$NAME$=$$,HLP.
CATALOG,RTLIBS,U,R.
ELSE,HLP.
NOTE./ type Pn ( n any pos. integer ) or P* for all.
NOTE./ type T to get to top, B to get to bottom
NOTE./ type Nn or N-n to move around in the file
NOTE,NR.* type END to exit XEDIT
LIBRARY.
RETURN,TXT.
GTR,RTLIBS,TXT.PROC/NAME
XEDIT,TXT,AS.
ENDIF,HLP.
```

EFFICIENT MATRIX PARTITIONING FOR OPTICAL COMPUTING

H.J. Caulfield, C.M. Verber, R.L. Stermer

I. Introduction

Many problems of data analysis, pattern recognition, and control can be stated as simple numerical linear algebra problem $m \times n$. Recent progress in optical numerical linear algebra [1-10] has led to the capability of constructing a very fast, low power, compact system for high accuracy calculations for any specific $m \times n$ matrix so long as m and n are not too large. The problem we address here is that while the dimensions of the problem is determined by the application, the dimension of the optical linear processor is determined by technological and economical constraints. The hypothesis we present is that any optical linear algebra problem of dimension $m \times n$ can be attacked with simple algorithms using processors of dimension $s \times s$. If this be true, the general problem reduces to identifying the set of simple algorithms, defining the rules of combination, and developing the devices required to perform the algorithms. With multiple $s \times s$ processors we can increase the overall solution speed through appropriate parallelism.

II. Criteria

Not all partitioning methods found in texts are satisfactory. Indeed some fail altogether while others are workable but poorly suited for these purposes. Accordingly, we offer here some criteria for choosing some methods over others.

First, the method should never require us to operate on a matrix of size greater than s. This obvious criterion eliminates a great many of the most famous matrix decomposition methods. Some matrix inversion methods, for instance, work by repeated division of matrices into four equal submatrices, finding the generalized inverse of the matrix in terms of those submatrices, decomposing each of the resulting submatrices into four equal submatrices, etc. until we reach easily invertable matrices. The final inverse is then reconstructed from the bottom up. The problem is that, for matrices of size $\geq 2s$, we reach matrix sizes larger than s. This, of course, defeates our original purpose.

Second, an ideal partitioning method for an optical computer would be extremely simple with little "bookkeeping" required. This reflects the fact that current optical computers are themselves very simple. They can do linear algebra but little else. A partitioning method which requires a great many non-optical side calculations would inevitably increase the time and hardware necessary to do the calculations.

Third, an ideal partitioning method would be application-independent. That is once we find the best algorithm for matrices of size $\leq s$, we want to use the same algorithm for a matrix of any size.

Fourth, we would like full efficiency in the partitioning scheme. For example, we would want a $2s \times 2s$ matrix to be solvable in four times the amount of time, T_0, needed for an $s \times s$ matrix. Furthermore with two modules we should reduce the time to $2T_0$. With four modules we should be able to achieve T_0 operation.

III. Suggested Method

We will describe here a partitioning approach which obviously meets the simplicity criterion. We will then show that it meets the other criteria as well.

The basic idea is that matrices and vectors can be partitioned into submatrices and subvectors which can be treated as ordinary numbers in carrying out operations. An example will show what we mean. Consider evaluation of the matrix-vector product $Ax = y$ where

$$A = \begin{bmatrix} a_{11} & a_{12} & a_{13} & a_{14} \\ a_{21} & a_{22} & a_{23} & a_{24} \\ a_{31} & a_{32} & a_{33} & a_{34} \\ a_{41} & a_{42} & a_{43} & a_{44} \end{bmatrix}, \qquad (1)$$

and

$$x^T = (x_1 \quad x_2 \quad x_3 \quad x_4). \qquad (2)$$

We might partition A and x into

$$A = \begin{bmatrix} A_{11} & A_{12} \\ A_{21} & A_{22} \end{bmatrix} \qquad (3)$$

and

$$x^T = [x_1^T \; x_2^T], \qquad (4)$$

where

$$A_{11} = \begin{bmatrix} a_{11} & a_{12} \\ a_{21} & a_{22} \end{bmatrix}, \tag{5}$$

$$x_1^T = (x_1, x_2). \tag{6}$$

etc.

Now

$$Ax = \begin{bmatrix} A_{11}x_1 + A_{12}x_2 \\ A_{21}x_1 + A_{22}x_2 \end{bmatrix} = \begin{bmatrix} y_1 \\ y_2 \end{bmatrix}, \tag{7}$$

where

$$y_1 = \begin{bmatrix} y_1 \\ y_2 \end{bmatrix} = A_{11}x_1 + A_{12}x_2 \tag{8a}$$

$$= \begin{bmatrix} a_{11} & a_{12} \\ a_{21} & a_{22} \end{bmatrix} \begin{bmatrix} x_1 \\ x_2 \end{bmatrix} \begin{bmatrix} a_{13} & a_{14} \\ a_{23} & a_{24} \end{bmatrix} \begin{bmatrix} x_3 \\ x_4 \end{bmatrix} \tag{8b}$$

$$= \begin{bmatrix} a_{11}x_1 + a_{12}x_2 + a_{13}x_3 + a_{14}x_4 \\ a_{21}x_1 + a_{22}x_2 + a_{23}x_3 + a_{24}x_4 \end{bmatrix} \tag{8c}$$

as we would have calculated using the full matrices. We have assumed that all matrices are padded with zero's if necessary so that m and n are multiples of s. Note that the four submatrix calculations needed can be performed in a way requiring a minimum of scratchpad memory. In fact, no scratchpad memory is needed if all the integration of vector components is done on detectors.

With a single $s = 2$ matrix-vector multiplier we would perform the two Y_1 multiplications first. The two operations we want to perform are those of eq. (8b). In figure 1 we show the engagement data flows for the two individual matrix-vector multipliers. In figure 2 we show how the two operations can be pipelined smoothly. After calculating y_1 and y_2 we would then calculate y_3 and y_4. Again the data flow can be pipelined as indicated in figure 3.

If we have two $s = 2$ modules available the two subvectors Y_1 and Y_2 can be calculated in parallel. This parallel calculation offers no problem in iterative operations since x is being supplied in parallel to the two modules. We simply start the Y_2 module two clock times after the Y_1 module as shown in figure 4. This is easily recognized as the data flow for an $s = 4$ module.

Finally, four $s = 2$ modules can be used in parallel to calculate y. The accumulation must be parallel to accomplish this. Parallel accumulation can occur optically by beam combining on detectors or electrically by simple summers.

Note that for a 4 x 4 matrix, a single $s = 2$ module takes longer than a single $s = 4$ module to perform a matrix-vector multiplication. On the other hand two $s = 2$ modules are equivalent to an $s = 4$ module and four $s = 2$ modules are faster than an $s = 4$ module.

Extensions to bigger s's and to matrix-matrix multiplication are quite trivial. All multiplier-accumulators available can be used efficiently either in a single large-s module or in many small-s modules. What counts in speed is the number of multiplier-accumulators available, so many small-s modules can calculate faster than a single large-s module if they are used in parallel. Data flow can always be organized to permit efficient feedback.

IV. Conclusion

We have shown that the simplest partitioning scheme is also the best on the basis of algorithm independence, minimum bookkeeping (i.e. suitability for optical computing), and efficiency. As a result we become problem-size independent in all concerns except speed and cost. The more multiplier-accumulators we devote to the problem the faster we solve it.

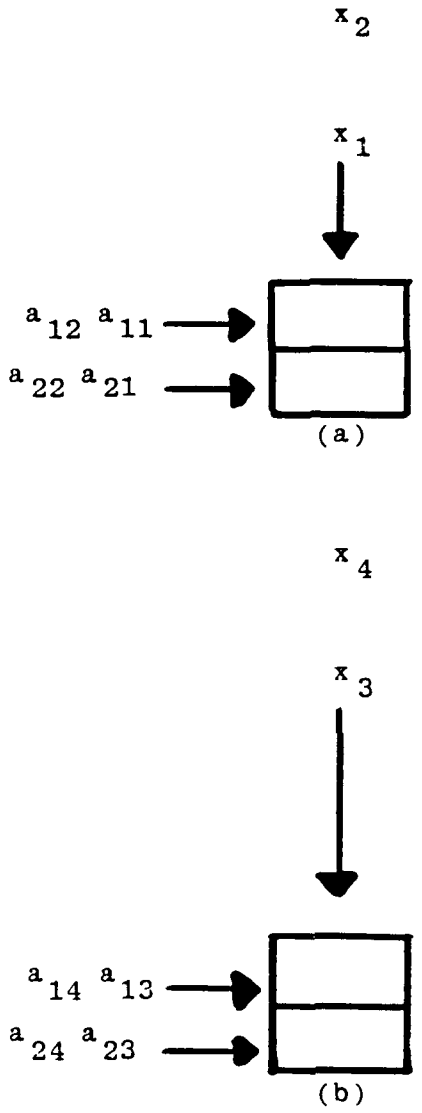

Figure 1

Data flow patterns for engagement processors doing the two $s = 2$ operations of eq. 8(b). The arrows indicate direction of flow in time. When two numbers meet they multiply and the products are accumulated in place.

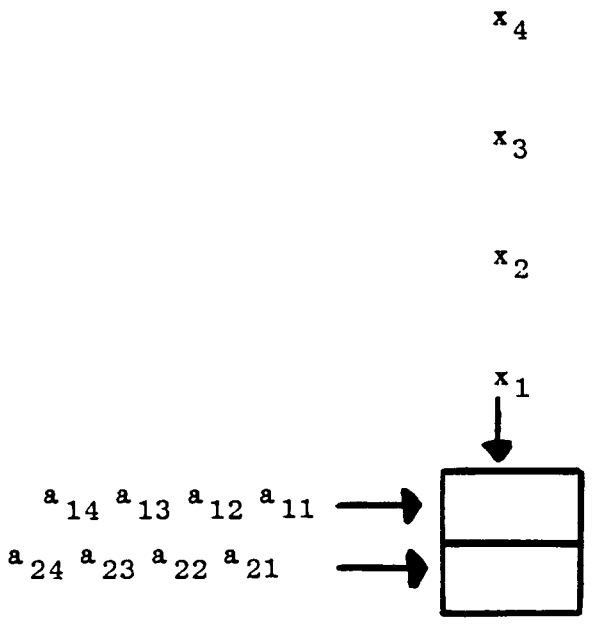

Figure 2

The two operations of figure 1 can be pipelined smoothly into one using the data flow shown here. The accumulated products will be y_1 and y_2.

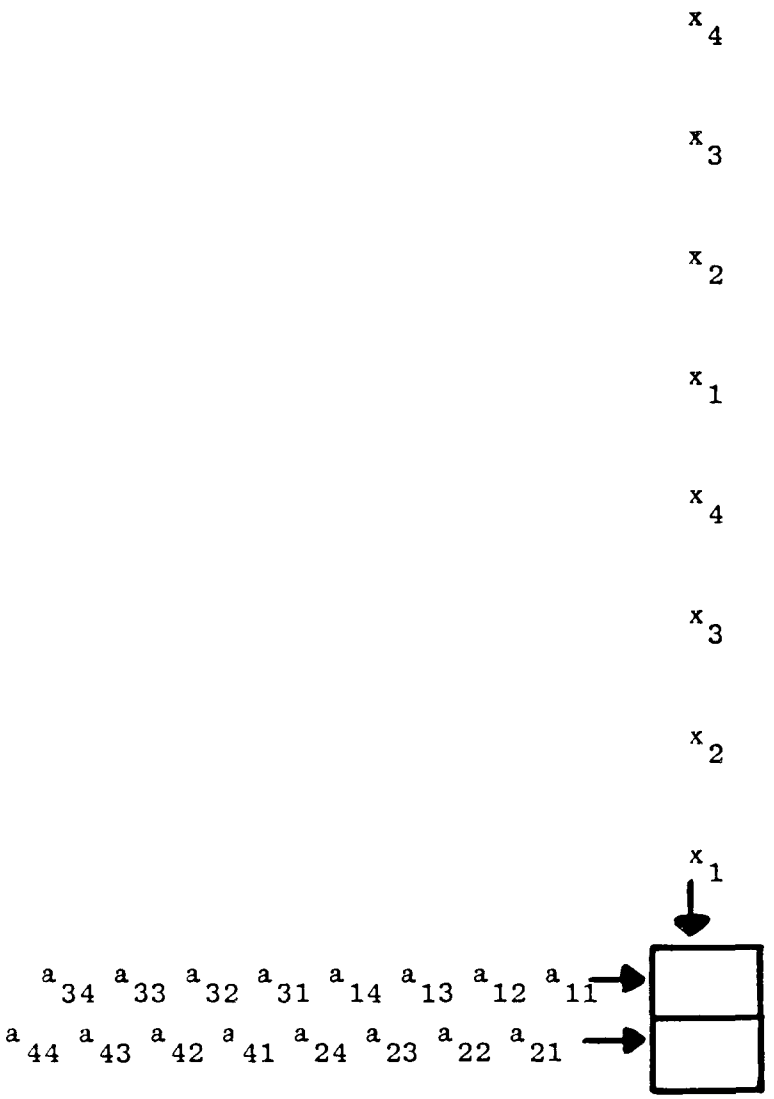

Figure 3

Pipelining of a single $s = 2$ engagement matrix-vector multiplier to do $Ax = y$ for the A and x of eqs. (1) and (2). The top accumulator produces y_1 (after 4 clock cyles) and y_3 (after 8 clock cycles). The bottom accumulator produces y_2 (after 5 clock cycles) and y_4 (after 9 clock cycles).

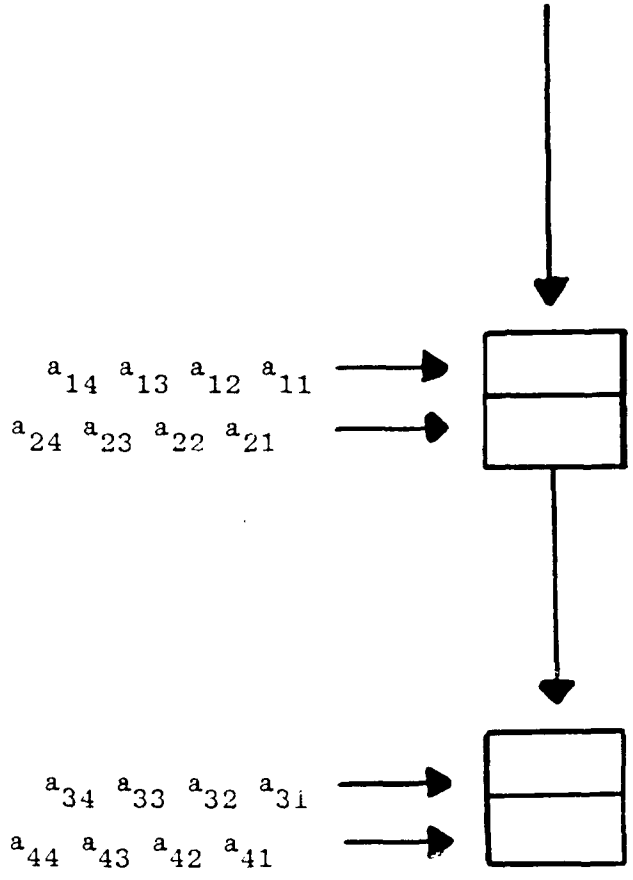

Figure 4

Two $s = 2$ modules can be pipelined to behave identically to an $s = 4$ module as shown here.

References

1. J.W.Goodman, A.R.Dias and L.M.Woody, Optics Lett. 2 (1978) 1.

2. D.Psaltis, D.Casasent and M.Carlotto, Optics Lett. 4 (1979) 348.

3. H.J.Caulfield, W.T.Rhodes, M.J.Foster and S.Horvitz, Opt. Comm. 40 (1981) 86.

4. R.A.Athale and W.C.Collins, Appl. Optics 21 (1982) 2089.

5. D.Casasent, J.Jackson and C.Neumann, Appl. Optics 22 (1983) 115.

6. R.P.Bocker, H.J.Caulfield and K.Bromley, Appl. Optics 22 (1983).

7. R.P.Bocker, Appl. Optics 16 (1983) 2401.

8. R.A.Athale, W.C.Collins and P.D.Stilwell, Appl. Optics 22 (1983) 365.

9. P.S.Guilfoyle, Opt. Eng. 23 (1984) 20.

10. R.P.Bocker, Opt. Eng. 23 (1984) 26.

FRINGE ORIENTATION DIFFRACTION EFFICIENCY IN BISMITH SILICATE

C. L. Woods, C. L. Matson[1] and M. M. Salour[2]
Rome Air Development Center, Solid State Sciences Division
Hanscom AFB, MA 01731

Introduction

We report the first experimental measurement of crystallographic orientation effects in the initial development of the diffraction efficiency of thick holograms produced by the photorefractive effect in a bismuth silicon oxide (BSO) crystal. Diffraction efficiencies of holograms made by interfering two plane waves on the (110) face are measured as a function of the angle between the fringe pattern and the applied voltage. Our measurements agree with the diffraction theory of a birefringent grating when optical activity is semi-quantitatively included. As the crystal is rotated relative to the interference fringes, the applied field may be adjusted to yield space charge dynamics with a constant growth time extending nearly into the steady state regime. The rotation-scaled applied electric fields and the crystallographic variations in the birefringent diffraction grating are both consistent with charge transport processes in which the initial space charge fields are perpendicular to the interference fringes.

Results

The optimum constant internal field electro-optic configuration of the BSO has been carefully studied for internal fields orientated normal to the electrodes.[3,4,5,6,7,8] Measurements presented here show

that these previous studies do not produce the optimum photorefractive grating diffraction efficiency. These measurements are tested relative to a new voltage scaling law and are in agreement with a simple relaxation model for the space charge field. The polarization dependence of the diffraction efficiency is semi-quantitatively analyzed by a diffraction of a partially pre-rotated (for optical activity) read beam incident on a birefringent grating.

In our experiment, three coplanar laser beams are incident on the BSO crystal, as shown in Figure 1. The two collimated 514.5 nm Ar^+ laser writing beams, polarized perpendicular to the optical table plane, produce a sinusoidal interference pattern of modulation index M, and have an average intensity of 5.0 W/cm^2 for the reported measurements. The half-intensity diameter of the write beams is twice the width of the crystal face. The modulation index is adjusted by varying the reflectivity of the read arm interferometer mirror. The modulation index, M, for the measurement reported is 0.82.

The dielectric mirror in the read arm of the interferometer is chosen to transmit the 632.8nm HeNe laser read beam which is used to measure the diffraction efficiency produced by the photorefractive effect. The half intensity diameter of the read beam is approximately 3mm (equal to the thickness of the crystal). The polarization of the read beam is selected to be either parallel or perpendicular to the fringe wave vector.

The interferometer producing the fringes is both compact and stable, with the path length of the two arms set equal to within a few millimeters. Increasing the fringe spacing of the writing pattern requires the lengthening and realignment of the two arms of the interferometer. These reported measurements are obtained with fringe

spacings of both 5 m and 3 m.

The BSO crystal (8mm x 8mm x 3mm) is cut and polished in the (110) transverse electro-optic orientation with electrodes attached with silver paste to the (110) edges of the crystal. The crystal had a 2^{o} wedge and is mounted on a rotating holder to adjust the azimuthal orientation of the fringes on the crystal. The crystal is rotated about the direction normal to the front face. Tilt adjustments allowed the back reflections of the write beams to be aligned.

As shown in the momentum vector diagram in Figure 1, a longer wavelength read beam, k_r, will have a larger angle of incidence on the crystal face to satisfy the Bragg diffraction condition. The read beam has a lower absorption in BSO, minimizing its effect on the space charge development. The read-write beam separation behind the crystal, together with the wavelength difference, allows the write beam energy to be well filtered and apertured out from the diffracted beam signal.

Write-measurements of the growth of the diffracted beam were obtained by opening a shutter blocking the Ar^{+} laser beam with an initial trigger from a stray write beam reflection. The previous space charge pattern was erased, the read beam power was minimized, and the read beam pre-exposure of the BSO (before the write beam illumination) was minimized. These measurement conditions produced stable, reproducible diffraction efficiency measurements.

The write measurements were stable up to the 200 ms. Diffraction efficiency measurements up to 100 ms are plotted in Figure 2, where the set of points for each angle is an average of 10 sequential measurements. The steady state measurement, however, exhibited relative fluctuations of a factor of 2. We will discuss only the

reproducible write-measurements in this report.

The data in Figures 2 through 4 was measured with the applied voltage, Va, increasing with the fringe angle according to the scaling law for the space charge field growth,

$$Va = \frac{Vo}{\cos\theta} \quad ,$$

where Vo is a constant and the fringe angle 0 is indicated in Figure 1. The data in Figure 2 is for the two polarizations of the read beam with M = 0.82, $\Lambda = 3\mu m$, and $I_o = 5.0\ mW/cm^2$. Table 1 gives the scaled applied voltage for various fringe angles for a Vo of 1 KV used in the data presented in Figure 2. The factors S_v and S_h are the multiplicative factors which must be removed to overlay the data at the different fringe orientation angles in Figure 2. The measurements for each polarization are adjusted relative to the 0^o data.

Comparison of the multiplicative shifts in Table 1 for different read polarizations, shows the dramatic behavior of the diffraction efficiency of polarized read beams. The opposite variation of the vertical and horizontal polarization diffraction efficiencies is emphasized by comparing the three-fold efficiency advantage of the horizontal relative to vertical polarization at an angle of 30^o, and the reverse thirty-fold efficiency advantage of the vertical relative to the horizontal polarization at a fringe angle of 75^o. In addition, linear polarized read beams have optimum polarizations for different fringe angle operating domains. For constant applied voltage, the horizontal polarization has nearly constant diffraction efficiency for fringe orientation from 0^o to 30^o, while the vertical polarization has a similarly uniform operating region for fringe orientation from 15^o

to 45°. There is, however, nearly an order of magnitude drop in diffraction efficiency for the vertically polarized read beam as the fringe orientation is increased from 0° to 15°.

The scaled voltage data in Figure 2 shows that the dynamics growth of the space charge is similar for angles studied. In contrast, measurements with the applied voltage held constant approach the steady state diffraction efficiency in less than a factor of two shorter time at fringe angles of 60°.

When using an unpolarized read beam with scaled crystal voltages, the read beam diffraction efficiency is constant to $\pm$ 50%. With a constant applied voltage and an unpolarized read beam, the diffraction efficiency drops off dramatically (by as much as two orders of magnitude) as the fringe angle is increased to 90°, with a trend somewhere between $\cos\theta$ and $\cos^2\theta$ for angles below 80°.

The data in Figure 2 may be compared with the model of the space charge growth as a simple relaxation process with time constant to a steady state value. The diffraction efficiency is proportional to the square of the sinusoidal space charge amplitude, and

$$\eta = \eta_{ss}(1-e^{-t/\tau})^2 \ .$$

The solid lines on Figure 2 are the curves for a time constant of 65 ms and agree with measurements for both read beam polarization to an accuracy of $\pm$ 8%.

A physical explanation for this angular space charge voltage scaling comes from examining the distance a photoexcited electron will be transported. If the space charge field is small relative to the applied field, an average drift distance $\mu\tau E$ projects a distance $\mu\tau E$

$\cos\theta$ normal to the fringe. For short times or for small values of the modulation coefficient, the internal space charge filled will be small relative to the applied field. And for thin windows of BSO, the field generated by charge drifting to (from) the 001 (top and bottom) surfaces will also be small. Values of the modulation coefficient near unity, however, produce a steady state space charge field with strong narrow peaks (strong spatial harmonics) with internal fields greater than the applied field.

The space-charge growth in a transverse-electrode photorefractive crystal illuminated by an interference pattern, with a wave vector, K, parallel to the applied field E have been calculated[4,5] and measured[3]. The charge transport model of Kukhtarev[4] may be utilized for any value of the fringe angle. A rotation of the direction of E will produce an angular dependence in the continuity equation by changing the current contribution from E to $E(\cos\theta)$, as long as the space charge contribution to the electric field is small relative to the applied field. The small space charge field approximation limit may be experimentally determined by rotating the fringes relative to the crystal and observing holographic diffraction efficiency growth at various angles while setting the voltage to keep the product $E(\cos\theta)$ constant. In Figure 2, additional departures from the scaled curves (at long times) indicate that a large space charge field is altering the charge transport. These experimental results indicate that the initial space charge field is perpendicular to the fringe interference pattern as indicated in Figure 1.

Figures 3 and 4 present direct experimental measurements of diffraction efficiency (defined by the ratio of the diffracted energy to the incident energy) plotted as a function of fringe angle at

constant growth times from 10ms to the steady state limit. For our measurements, the steady state diffraction efficiency was a time average of an unstable value, varying by about a factor of two. Other measurements have the error bars indicated in the figures. The data in both figures was obtained with the scaled voltages listed in Table 1, a modulation index of 0.82 and an interference fringe spacing of 5μm. Since diffraction efficiencies are directly plotted, a comparison of the vertically polarized read beam measurements in Figure 3 with horizontally polarized read beam measurements in Figure 4 illustrates the substantial differences indicated by the multiplicative factors in Table 1.

The space charge electric field (Figure 1) will change the local index ellipsoid of the BSO, producing a thick birefringent diffraction grating in an optically active crystal. A semi-quantitative model of this diffration is obtained by separating the birefringent grating and optical activity into serially produced effects, as has been done with constant internal fields in BSO.

BSO crystals are cubic with no inversion symmetry and belong to point group 23 and have two orientations in which the electro-optic effect is purely transverse--the (111) and (110) orientations as discussed for PROM and PRIZ devices by Petrov and Khomenko[7]. The crystal sample studied in this experiment was of (110) orientation with electrodes on the other (110) faces. When no electric field is applied, the crystal is optically isotropic. With an applied electric field, the three non-zero elements of the electro-optic tensor are equal and distort the crystal index ellipsoid in one of the simplest manners. In the (110) orientation, the index of refraction change is maximized and the principal axes of the index ellipsoid are

perpendicular to the (110) entry face and along the two face diagonals (for electric fields along the transverse 110 direction).

Expanding the change in the index of refraction produced by an internal space charge field generating a total internal field at an angle γ relative to the (001) axis in terms of differential changes in the magnitude (ΔE) and orientation ($\Delta\gamma$) of the total internal field (Figure 1) one obtains the following expressions for the changes along the face diagonal principal axis x' and y':

$$\frac{\Delta n}{n_o} = 1/2\eta_o^2 r E_a\left(1 + \frac{\Delta E}{E} + \Delta\gamma\right), \text{ along x', and}$$

$$\frac{\Delta n}{\eta_o} = -\,1/2\eta_o^2 r E_a\left(1 + \frac{\Delta E}{E} - \Delta\gamma\right), \text{ along y'.}$$

The change in the index of refraction along the principal axes is expressed in terms of the zero field index of refraction, n_o; the electro-optic coefficient, r; the applied field, Ea; and first order changes in the orientation of the internal field and its magnitude.

For Es normal to the fringe pattern and a scaled applied voltage, the relative changes in the diffraction efficiency are compared with experimental measurements in Figures 3 and 4. An empirical 35^o polarization rotation has been applied to the vertically polarized (perpendicular to the fringe wave vector) data in Figure 3, and an empirical 20^o polarization rotation has been applied to the horizontally polarized (parallel to the fringe wave vector) data in Figure 4. The polarization rotation for a 632.2nm beam passing through 3m of BSO is 66^o. The empirical correction applied in Figures 3 and 4 are 1/3 to 1/2 of the total rotation, corresponding to an average during transmission.

As indicated in Figure 3 and 4, this approach provides a

semi-quantitative agreement with experiment. The order of magnitude variations in the diffraction efficiency are in $\pm$ 50% agreement with this theory.

These measurements in BSO show that a single relaxation rate model for the space charge is in good agreement well into the intermediate growth region, that the fringe angle voltage scaling is accurate over this same time range, and that the polarization dependence of the photorefractive diffraction can be semi-quantitatively modeled by a birefringent grating with incident light at a rotated polarization angle to account for the effective optical activity of the crystal.

Table 1 Scaled Applied Voltages and Multiplicative Shifts For Figure 2

Point Label	θ	Va (kV)	S_v	S_h
A	0°	1	1.0	1.0
B	15°	1.04	no data	1.36
C	30°	1.15	0.64	1.91
D	45°	1.41	1.75	1.16
E	60°	2.00	1.60	0.21
F	75°	3.86	1.43	0.052
G	78.5°	5.00	0.93	0.080

FOOTNOTES

1. Air Force Institute of Technology, Wright Patterson AFB, OH 45433.

2. TACAN Aerospace Corporation, 2111 Palomar Airport Road, Carlsbad, CA 92008.

3. J.P. Huignard and F. Micheron, Appl. Physics Letter 29, 591 (1976).

4. N.V. Kukhtarev, V.B. Markov, S.G. Odulov, M.S. Soskin and V.L. Vinetskii, "Holographic Storage in Electro-Optic Crystals," Ferroelectrics, 22, 949 (1979).

5. M.G. Moharam, T.K. Gaylord, R. Magnusson and L. Young, J Appl. Physics, 50, 5642 (1979).

6. J.P. Herriau, J.P. Huignard, and P. Aubourg, App. Optics 17, 1851 (1978).

7. M.P. Petrov and A.V. Khomenko, Sov. Phys. Solid State, 23 789 (1981).

8. Y. Owechko and A.R. Tanguay, Jr., Opt. Comm. 44, 239 (1983).

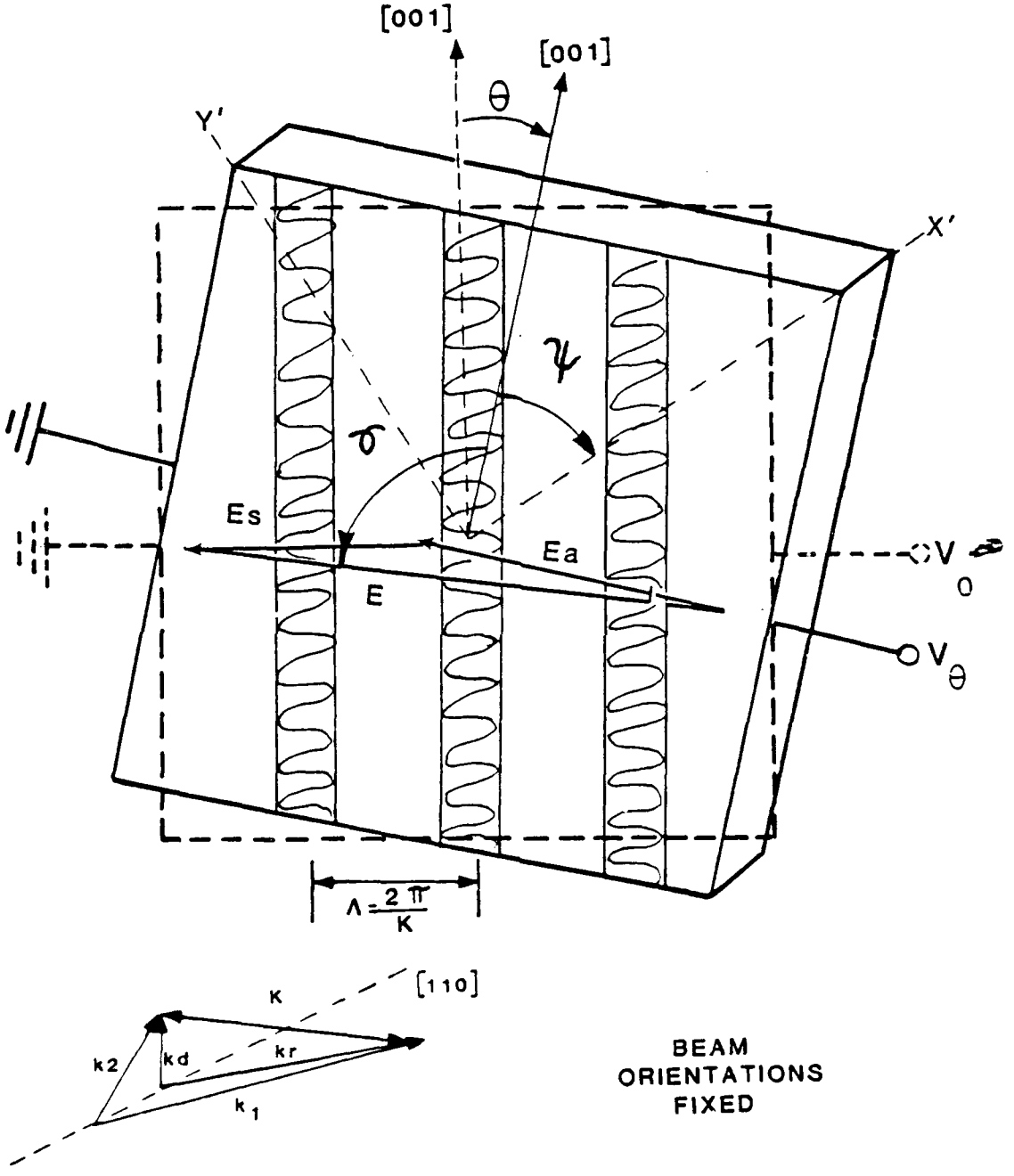

CRYSTALLOGRAPHIC ORIENTATION OF CUBIC BISMUTH SILCON OXIDE CRYSTAL SAMPLE WITH MOMINTUM VECTOR DIAGRAM FOR WRITE & READ BEAMS

FIGURE 1

FIGURE 2

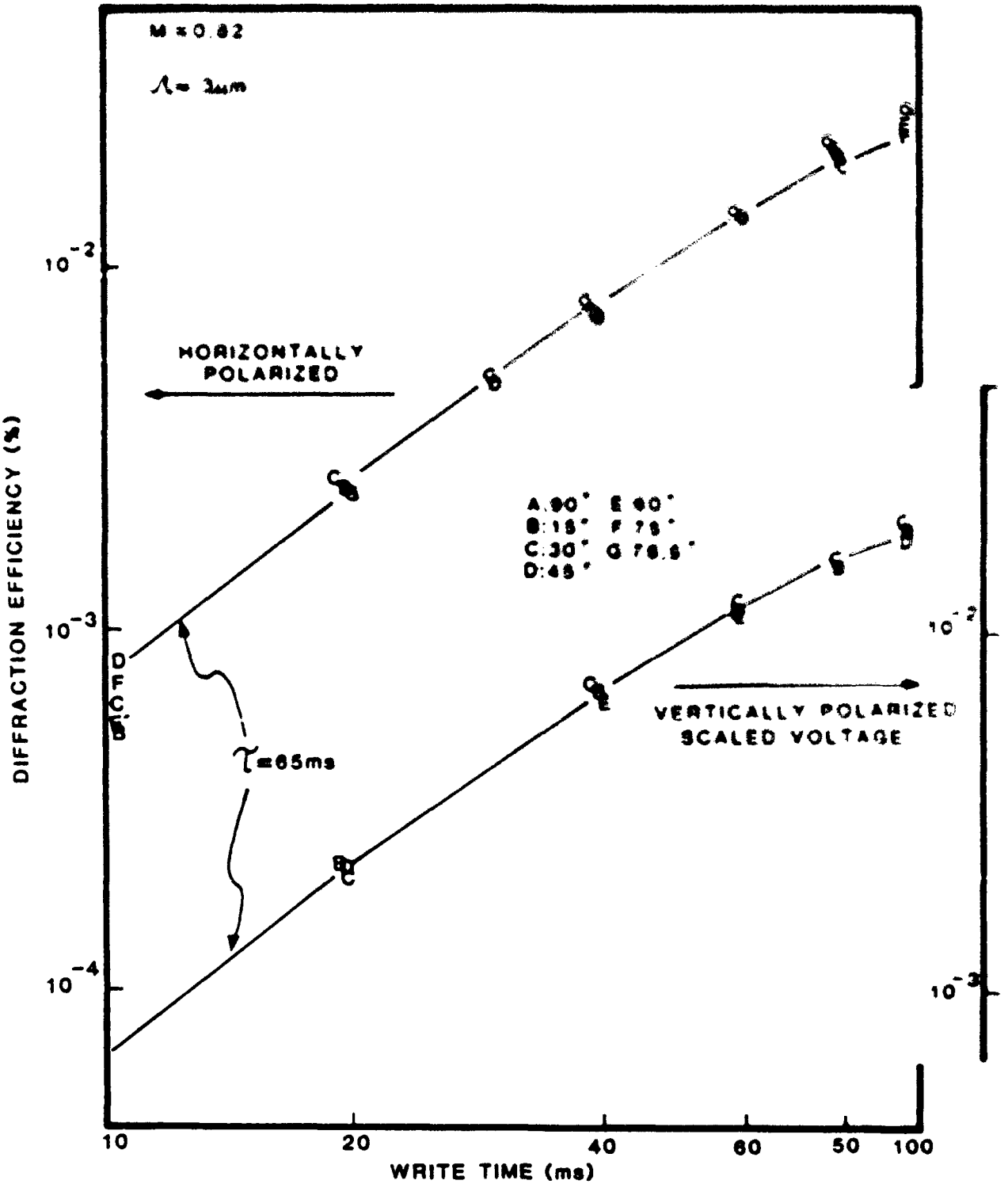

DIFFRACTION EFFICIENCY VERSUS WRITE TIME WITH THE MEASUREMENTS AT EACH ANGLE SCALED RELATIVE TO THE $\theta = 0°$ MEASUREMENTS

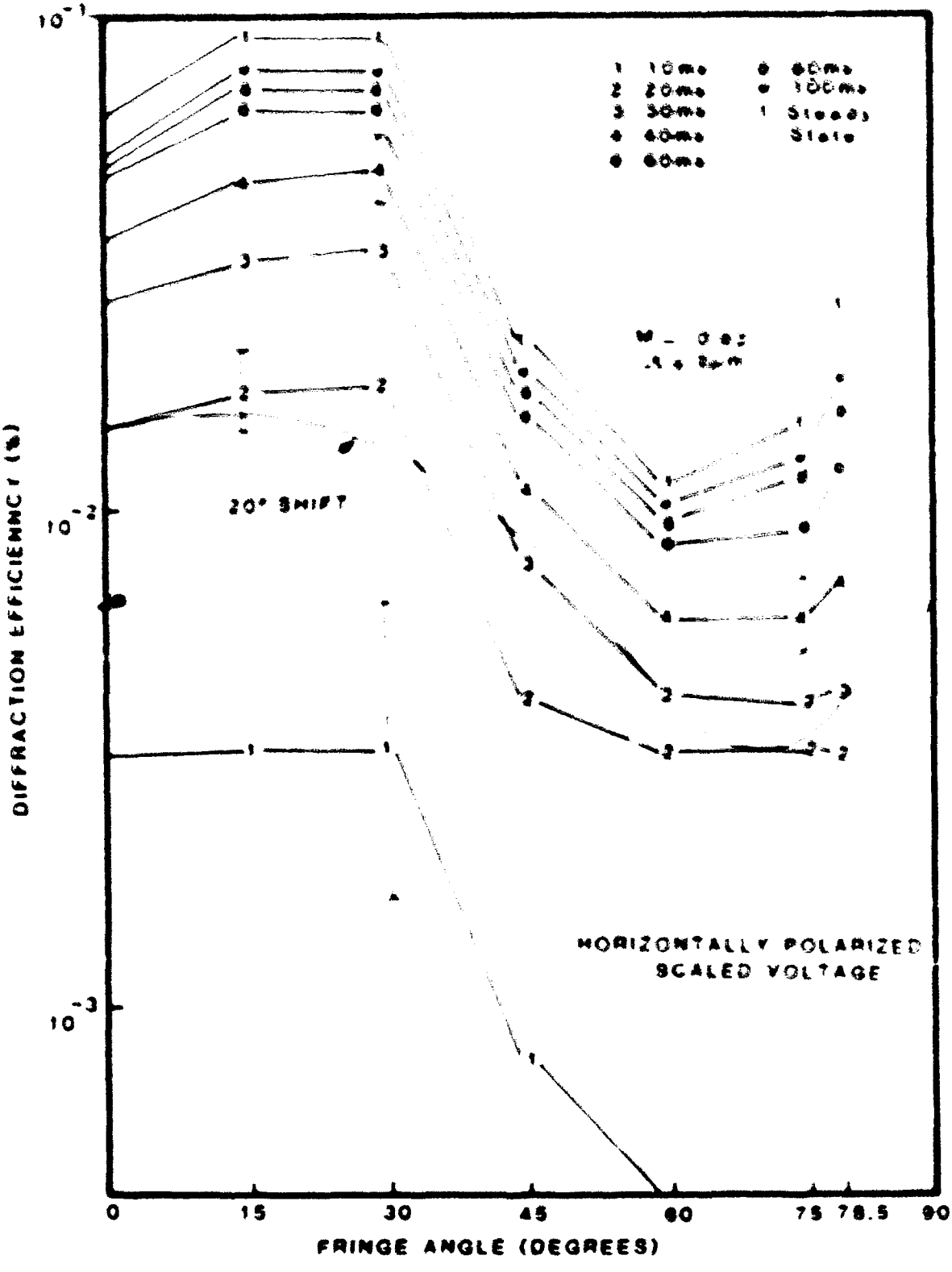

DIFFRACTION EFFICIENCY VERSUS FRINGE ANGLE WITH WRITE-TIME AS A PARAMETER, COMPARED WITH THE 20° SHIFT OF THE BIRIFRINGENT THEORY

FIGURE 4

MISSION
of
Rome Air Development Center

RADC plans and executes research, development, test and selected acquisition programs in support of Command, Control, Communications and Intelligence (C^3I) activities. Technical and engineering support within areas of competence is provided to ESD Program Offices (POs) and other ESD elements to perform effective acquisition of C^3I systems. The areas of technical competence include communications, command and control, battle management information processing, surveillance sensors, intelligence data collection and handling, solid state sciences, electromagnetics, and propagation, and electronic reliability/maintainability and compatibility.